Fifty Years of Inorganic Biomimetic Chemistry: From the Complexation of Single Metal Cations to Polynuclear Metal Complexes by Multidentate Thiolate Ligands

Josef Taut, Jean-Claude Chambron, Berthold Kersting

EurJIC
European Journal of Inorganic Chemistry

Review
doi.org/10.1002/ejic.202200739

Chemistry Europe
European Chemical Societies Publishing

www.eurjic.org

Fifty Years of Inorganic Biomimetic Chemistry: From the Complexation of Single Metal Cations to Polynuclear Metal Complexes by Multidentate Thiolate Ligands

Josef Taut,[a, b] Jean-Claude Chambron,*[b] and Berthold Kersting*[a]

This article covers 50 years of coordination chemistry of transition metal complexes and metal-sulfur aggregates involving thiolate-incorporating ligands by reviewing selected examples. The studies in the coordination chemistry of sulfur-rich ligands have been undoubtedly triggered and fed by the concomitant development of bioinorganic chemistry, particularly of iron-sulfur enzymes. The review is broken down in five sections, which examine complexes of increasing nuclearity, including binuclear complexes based on compartmental macrocyclic ligands. We show also how ligand engineering has allowed the researchers in the field to control the nuclearity of the complexes, which was a particularly difficult task for sulfur-based ligands, as thiolates show a strong tendency to coordinate to more than one metal cation at once.

1. Introduction

Nature shows numerous examples of metalloproteins and metalloenzymes that are found in all types of organisms, from archae to eukaryotes, and that involve metal cations bound at least to a thiolate ligand RS^-, in general from a cysteine residue, or to sulfide S^{2-}, the latter playing the role of a bridging monoatomic, dianionic ligand. Thiolate shows also a particular ability to bridge several metal cations. Compared to other biologically-relevant ligands, such as those based on oxygen and nitrogen donor atoms, thiolate ligands are softer but stronger electron donors, transferring higher electron density on the bound metal cation, and the metal-thiolate bond has a higher covalent character. Another pecularity of metal bound thiolate is its ability to undergo protonation.[1] Thiolate ligands may also stabilize metal ions in high oxidation states. However, due to their "non-innocent" character ligand-based oxidations may occur, and this complicates the interpretation of the observed redox properties.[2,3] Metal-thiolate complexes often display intense colors due to allowed thiolate-to-metal charge transfer transitions.[4] The formation of aggregates or polymers with poor solubility and lack of integrity is often seen in the chemistry of simple alkyl thiols.[5] This drawback can be avoided by utilising sterically more demanding ligands such as thiophenols with alkyl groups in the ortho-positions to the sulfhydryl function. Juxtaposing the thiolate donor atoms together with additional donor atoms (which block open coordination sites) within a macrocyclic framework is also a powerful strategy to control the nuclearity of the resulting complexes.[6,7] Most thiolate ligands are sensitive to oxidation by air oxygen, particularly in their deprotonated state, and this often hampers working with thiolate ligands. Use of appropriate methods (glovebox, Schlenk techniques) that guarantee O_2-free conditions is necessary in order to avoid the unwanted formation of the various oxidation products (disulphide, sulphenate or sulphinate).[8] The consequence of these characteristics of the metal-sulfur bond is its involvement in metalloproteins showing a large diversity of functions, such as: Cu and Zn transport and storage, toxic metal (Cd) sequestration and removal by metallothioneins;[9] electron transfer by ferredoxins (proteins containing iron-sulfur clusters) and cupredoxins (proteins containing a type I copper center).[10] Other metalloproteins are involved in the catalysis of many biochemical reactions, most of them using small molecules: redox catalysis, such as in the case of dihydrogen (redox processes involving H_2/H^+ performed by hydrogenases),[11] dioxygen (O_2 reduction to superoxide and monooxygenase activity by cytochrome P450),[12] superoxide (dismutation into hydrogen peroxide and oxygen by nickel superoxide dismutase),[13] carbon monoxide (concomitant oxydation of CO to CO_2 and reduction of an electron acceptor by water performed by carbon monoxide dehydrogenase),[14] nitrous oxide (reduction of N_2O into dinitrogen by nitrous oxide reductase),[15] and dinitrogen (reduction of N_2 into ammonia by nitrogenases);[16] Lewis acid catalysis, such as in the case of the conversion of nitrile into amide (Fe or Co nitrile hydratase)[17] and oxydation of alcohols to aldehydes and ketones (Zn alcohol dehydrogenase),[18] just to mention a few. Unsurprisingly, most of the redox processes catalyzed by sulfur-rich metalloenzymes

[a] J. Taut, Prof. Dr. B. Kersting
Institut für Anorganische Chemie
Universität Leipzig
Johannisallee 29, 04103 Leipzig (Germany)
E-mail: b.kersting@uni-leipzig.de
https://www.chemie.uni-leipzig.de/en/institut-fuer-anorganische-chemie/kersting-group
[b] J. Taut, Dr. J.-C. Chambron
Institut de Chimie de Strasbourg
UMR 7177 CNRS-Université de Strasbourg
1, rue Blaise Pascal, 67008 Strasbourg (France)
E-mail: jcchambron@unistra.fr
https://lclac.chimie.unistra.fr/

Review
doi.org/10.1002/ejic.202200739

are reductions combined with proton transfer processes. We shall examine now in more detail the active centers of the metalloproteins exhibiting the highest sulfur-to-metal ratio, that is, those containing [Fe–S] clusters. These include the various ferredoxin electron transfer proteins, but also metalloenzymes involving [Fe–S] clusters, such as the nitrogenases,[19] or metalloenzymes involving a [Fe–S] cluster in the proximity of a metal complex subunit in a mixed thiolate environment, such as the hydrogenases,[11] acetyl coenzyme A synthase (ACS) and carbon monoxide dehydrogenase.[14] In addition, hydrogenases and nitrogenases are very important metalloenzymes as far as the hydrogen economy is concerned. The hydrogenases represent the solution nature has found to use dihydrogen as a molecular reductant; the nitrogenases, which can work as hydrogenases in the absence of dinitrogen,[20f] perform the reduction of dinitrogen into ammonia, one of the sources of nitrogen for the synthesis of aminoacids, in very mild conditions, while the industrial production of ammonia relies on the extremely energy consuming Haber-Bosch process. Therefore, in a period where it is time to switch from an oil-based economy to an electricity-based economy, it would be very important to mimic nature.[20]

In iron-sulfur proteins the [Fe–S] aggregates or clusters are held by the thiolate residues of several of the cysteine amino acids that are part of the backbone of these proteins (Figure 1). If we except the case of mononuclear rubredoxin[21] (Figure 1a), in which the Fe^{2+} cation forms a complex of tetrahedral coordination geometry with the thiolate residues of four cysteine amino-acids, which can be formulated $[Fe(Cys)_4]^{2-}$, the smallest iron-sulfur active sites are those of the dinuclear ferredoxins[22] and the Rieske protein,[23] which correspond to the formulae $[Fe_2S_2(Cys)_4)]$ (Figure 1b) and $([Fe_2S_2(Cys)_2(His)_2)]$, respectively. In each complex the metal centers display a tetrahedral coordination geometry. As a result, the central plane formed by the $[Fe_2S_2]$ diamond is orthogonal to the side planes defined by the cysteinyl sulfur atoms and the iron cation they are bound to. Ferredoxins,[10] as well as the HiPIP (High reduction Potential Iron-sulfur Protein),[24] also contain $[Fe_4S_4]$ aggregates. The iron-sulfur clusters have a highly deformed cubic structure the vertices of which are occupied alternatively by the Fe cations and the sulfide dianions (Figure 1c). The roughly tetrahedral coordination sphere of each Fe cation is completed by the thiolate residue of a cysteine amino acid. HiPIP and ferredoxins are electron transfer proteins, which can be found in the protein machinery of bacterial and plant photosynthesis. There are also $[Fe_4S_4]$ aggregates that are part of metalloenzymes, i.e. metalloproteins performing a chemical transformation, such as quinolinate synthase,[25] and nitrite[26] and sulfite[27] reductases, just to mention additional enzymes. Noticeably, in the latter, one of the four iron cations is connected to the Fe center of the so-called siroheme through a sulfide bridging anion, which makes it different from the three others. Other examples of low nuclearity metalloenzymes are the already mentioned hydrogenases that reduce two protons into dihydrogen and vice-versa (Figure 1d).[4] The active site H of the hydrogenases contains two metal cations, both iron in [FeFe] hydrogenases,[28] a nickel and an iron cation in [NiFe] hydrogenases (Figure 1h).[29] The coordination sphere of the Fe^{2+} cation is completed by two cyanide anions and carbon monoxide. In the resting state (Ni-SI_a) of the [NiFe] hydro-

Josef Taut was born in Leipzig, Germany in 1995. He graduated in chemistry in 2021 from the University of Leipzig, where he is currently pursuing PhD studies in the groups of Prof. Dr. B. Kersting and Prof. Dr. Abel. During his studies he had the opportunity to work at the ETH Zürich. He is currently doing a research internship at the University of Strasbourg. His research interests are in supramolecular coordination chemistry, nanoparticles and biochemistry

Jean-Claude Chambron has been a CNRS Research Director since 1999. He worked for his PhD under the supervision of Prof. Dr. Jean-Pierre Sauvage. After postdoctoral studies at UC Berkeley, he returned in Strasbourg as a CNRS research associate, working on topological chirality and porphyrin-incorporating catenanes and rotaxanes. In 2001 he moved to the University of Burgundy (Dijon), where he carried out research in supramolecular chemistry (chirality induction, sensing, and self-assembly of chiral molecular cages), and in the development of chelators for radioactive tetravalent metals with applications in molecular imaging. He holds his current position at the Institute of Chemistry of Strasbourg since 2018.

Berthold Kersting got his doctoral degree from the University of Münster with Prof. Dr. Bernt Krebs in 1993. He did postdoctoral studies with Ken Raymond at UC Berkeley (1994-1995). He carried out his habilitation at the Institute of Inorganic and Analytical Chemistry of the University of Freiburg, working on the coordination chemistry of dinuclear transition metal complexes supported by macrocyclic amino-thiolato ligands. Since 2004 he is Professor of Inorganic Chemistry at the University of Leipzig. His research interests focus on supramolecular coordination chemistry, molecular magnetism, and bioinorganic chemistry.

Review
doi.org/10.1002/ejic.202200739

Chemistry Europe
European Chemical Societies Publishing

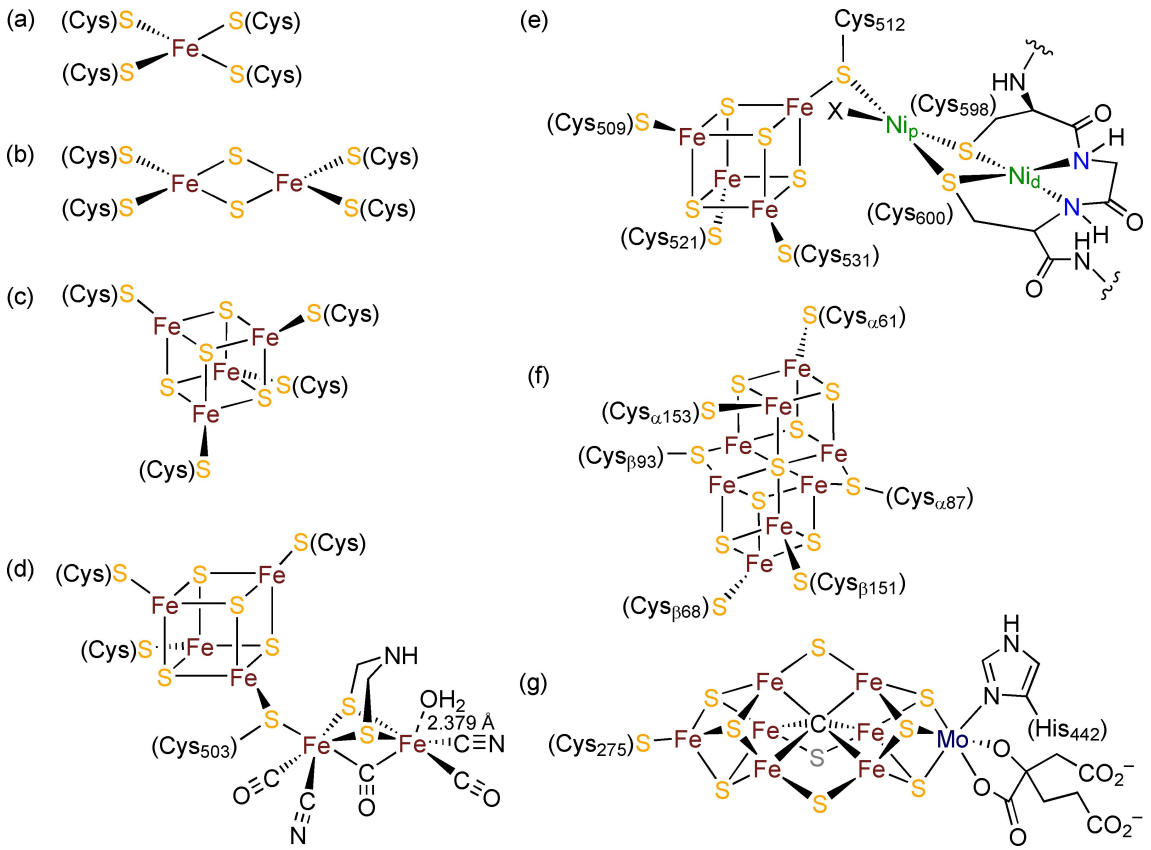

Figure 1. Schematic structures of the active centers (charges omitted) of (a) mononuclear (b) dinuclear and (c) tetranuclear ferredoxins, (d) the [FeFe] hydrogenase from *Clostridium pasteurianum*,[27a] (e) the acetyl-CoA synthase from *Carboxydothermus hydrogenoformans*,[29a] (f) the P (P^N state) cluster of the nitrogenase of *Klebsiella pneumoniae*,[31d] and the (g) M cluster (FeMoco) of the nitrogenase from *Azotobacter vinelandii*.[32]

genases the Ni^{2+} cation is bound two four cysteinyl thiolates, two terminal ones and two that hold the two metal cations together. This state is able to trigger the heterolytic cleavage of H_2, producing the state Ni–R in which the metal cations are further bridged by the hydride anion. The initial Ni-SI_a state is restored after release of two protons and two electrons. Noticeably, in the [FeFe] hydrogenase, the cysteinyl thiolate bound to one of the Fe atoms is also connected to an $[Fe_4S_4]$ cluster, which makes the $\{[Fe_4S_4]S(cys)\}^-$ ensemble a redox variable metallothiolate ligand. Similar metallothiolate ligands are also involved in metalloenzymes such as acetyl coenzyme A synthase and carbon monoxide dehydrogenase.[14] In ACS, the catalyst for the CO/CH_3 coupling reaction is multimetallic (A cluster) and can be formulated as $[N2S2]Ni_dM'_pS(cys)[Fe_4S_4]$, the $[N2S2]Ni_d$ playing the role of a complex-as-ligand for M'_p (Figure 1e).[30] Depending on the origin of the enzyme, M'_p was identified as $Cu^{(I)}$ or $Zn^{(II)}$ in an $[(\mu\text{-}S)_3L]$ tetrahedral geometry (all three $\mu\text{-}S^-$ thiolate provided by a metal-bound cysteine, including two from [N2S2]Ni), or $Ni^{(II)}$ in a $[(\mu\text{-}S)_3L]$ square-planar geometry. Chelation of the single metal cation M found in the active sites of ACS and carbon monoxide dehydrogenase through thiolate sulfur and amido nitrogen is secured by the tripeptide sequences Cys-X-Cys, where X = glycine and M = Ni. The [N2S2]M complex subunit is also found in the active site of nitrile hydratase (X = serine; M = Co or Fe), which lacks a proximal $[Fe_4S_4]$ cluster.

We shall now focus on nitrogenases, in particular the molybdenum nitrogenase, which represents another example of reducing enzyme, but at a more complex level, as it converts dinitrogen into ammonia (the so-called fixation of N_2), which is a 6 H^+, 6 e^- process.[16,31] Nitrogenase is particularly relevant because of the diversity of iron-sulfur clusters, in particular of higher nuclearity than four it involves. Nitrogenase is a complex of two proteins: The "Fe protein" in which an $[Fe_4S_4]$ cluster bridges a protein dimer, each component incorporating a nucleotide triphosphate hydrolase;[31b] the "MoFe" protein, an $\alpha_2\beta_2$ tetramer, each $\alpha\beta$ subunit incorporating two high nuclearity [Fe–S] clusters. The P cluster (Figure 1f) can be considered as resulting from the fusion of two $[Fe_4S_4]$ clusters that share a sulfide vertex. Two iron cations of each $[Fe_4S_4]$ subunit that are directly bound to the shared S^{2-} anion are, in addition, bridged by a cysteinyl thiolate residue, therefore the P cluster is held by the protein through six cysteinyl thiolates. The role of the P cluster is to convey electrons from the Fe protein to the M cluster (FeMoco). In this context, it is important to note that the topology of the cluster changes with is oxidation state, as in the P^{OX} form two Fe–S bonds of one of the $[Fe_4S_4]$ subunits are disrupted by comparison with the all-ferrous P^N form.[31c] The M cluster (Figure 1g) is the catalytic site of the

Review
doi.org/10.1002/ejic.202200739

metalloenzyme, where the reduction of dinitrogen to ammonia takes place. It differs in many points from those examined until now, in particular by the fact that, in addition to the iron, it contains a Mo cation. It can be described as the result of the fusion of a $[Fe_3S_3]$ cluster and a $[MoFe_2S_3]$ cluster at a central atom, which was relatively recently identified as a carbide anion.[32] The distal Fe and the Mo cations occupy the vertices at the extremities of the cluster and are the only cations bound to the protein through a cysteinyl sulfide for Fe and an histidinyl nitrogen for Mo. In addition to being bound to C^{4-} the six central iron cations are connected pairwise by S^{2-} bridges. It is important to note that, whereas the structure of the P cluster in the P^N state could be reproduced synthetically,[33] the M cluster resisted so far all attempts of synthesis of structural analogues, and, in spite of a plethora of experimental and theoretical studies, a complete, fully accepted mechanism is still awaited.[34]

This very short overview on natural iron-sulfur aggregates found in metalloproteins shows that one of the roles of the protein is that of a multidentate ligand, mainly thiolate (cysteinate) in the present case. This is particularly true in the case of metallothioneins. Besides providing an environment with suitable properties in terms of hydrophobicity/hydrophilicity, acid/base and redox properties, another role of the protein is to position the active sites at the right distance and the right orientation.[35] Biomimetic chemistry aims at modelling the structure and the function of metalloproteins by focusing on the active site, using synthetic multidentate ligands that are able to provide the same coordination environment as the protein. As examples among the very large body of works in this area we shall only mention the pioneering works of Holm on the [Fe–S] clusters.[36] By contrast, the complexation of a single metal cation by thiolate ligands was not an easy task, because of the high propensity of thiolates to act as bridging ligands. Therefore, several strategies were devised in order to force the thiolate to coordinate only one metal center. These approaches are discussed first (section 2). Then we shall examine model complexes of increasing nuclearity: Binuclear systems are examined both in sections 3 and 4, the latter focusing on macrocyclic systems, which was a very fruitful and efficient approach to the controlled formation of $[M_2S_2]$ motifs. In section 5 the historical development of the coordination chemistry of the $[Fe_4S_4]$ clusters is presented with emphasis on the subsite differentiation of one Fe atom with respect to the remaining three. The success of the biomimetic approach relied on the development of preorganized ligands featuring three thiolate donors. In the end of this section, we provide one example of the strategies for making high nuclearity [Fe–S] clusters, like those found in nitrogenases. Finally, section 6 shows several examples of metal-thiolate aggregates of nuclearity greater than four that are incorporated in macrocycles or are stabilized by several macrocycles or metallamacrocycles.

2. The Complexation of a Single Metal Cation by Thiolate Ligands

Basically, two directions were taken for the design of suitable thiolate ligands for the coordination of a single metal cation: (i) sterically-hindered monodentate or bidentate ligands; (ii) small tripod ligands.

2.1. Sterically-hindered monodentate thiolate ligands

An alternative to small tri-thiolate ligands for the formation of low coordinate $Fe^{(II)}$ complexes was investigated by Power and coworkers, who used sterically hindered arylthiolates by 2,6-substitution. While this substitution does not prevent the formation of binuclear complexes involving bridging arylthiolate ligands, such complexes can be used as precursors for the generation of tricoordinate arylthiolate $Fe^{(II)}$ complexes. Accordingly (Figure 2), reaction of $[Fe_2(SC_6H_2\text{-}2,4,6\text{-}(t\text{-}Bu)_3)_4]$ **1** with 2 equiv. of 2,4,6-$(t\text{-}Bu)_3C_6H_2S^-$, followed by the addition of PPh_4Cl afforded the mononuclear anionic complex $(PPh_4)[Fe(SC_6H_2\text{-}2,4,6\text{-}(t\text{-}Bu)_3)_3]$ **2** in which the Fe^{2+} cation exhibits a slightly distorted trigonal planar geometry with idealized C_{3h} symmetry for the $Fe(SC_{ipso})_3$ array. Mössbauer spectroscopy studies indicated that the trigonal planar $[Fe(SAr)_3]^-$ could be

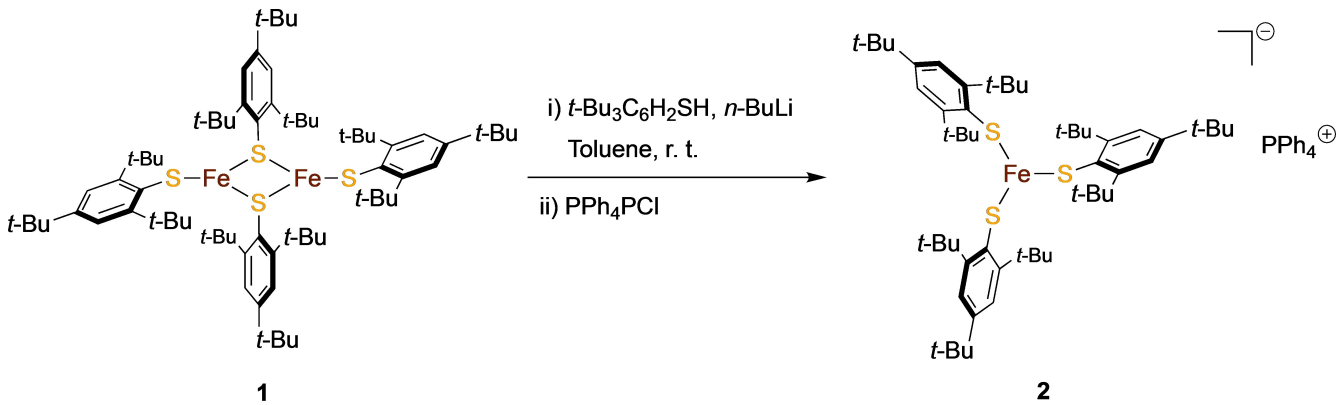

Figure 2. Rearrangement of a dinuclear $Fe^{(II)}$ complex with four sterically hindered arylthiolate ligands including two bridging ones into a mononuclear $Fe^{(II)}$ tri-thiolate complex.[37]

distinguished from tetrahedral $[Fe(SAr)_4]^{2-}$ analogues on the basis of its smaller quadrupole splitting at temperatures < 100 K.[37]

The concept of sterically-hindered monodentate thiolate ligands was also exploited by Millar and Koch to synthesize $[Fe^{(III)}(SR)_4]^-$ complexes as models of the oxidized form of the $[Fe(S\text{-}cys)_4]$ center of rubredoxin without oxidation of the thiolate to disulfide.[38] As a matter of fact, the use of thiolates such as those derived from 2,3,5,6-$(Me)_4C_6HSH$ and 2,4,6-$(i\text{-}Pr)_3C_6H_2SH$ allowed these authors to isolate the corresponding complexes in high yields. Remarkably, the D_{2d} symmetry of the $[FeS_4]$ core in the X-ray crystal structure of [Fe(2,4,6-$(i\text{-}Pr)_3C_6H_2S)_4$] **3** is a characteristic of the $[FeS_4]$ cores of rubredoxins, as shown by the analysis of the X-ray crystal structures of five different rubredoxins (Figure 3).

2.2. Sterically-hindered dithiolate chelates

Holland and coworkers reported the *meta*-phenylene bridged bis-(*o*-thiophenolate) chelate $\mathbf{L1}^{2-}$ in which the sulfur atoms are flanked by bulky 2,4,6-tri(isopropyl)phenyl substituents in order to isolate complexes of 1:1 stoichiometry only (Figure 4).[39] Accordingly, the complex $[Fe^{(III)}(\mathbf{L1})(THF)_2]$ could be isolated and

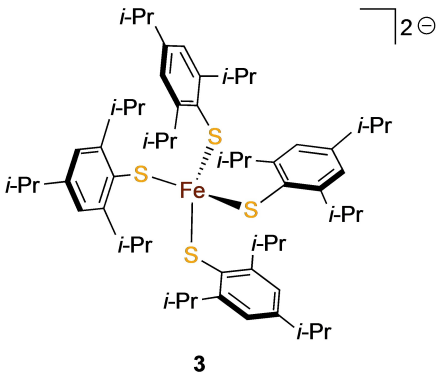

Figure 3. View of the molecular structure of the synthetic model of a rubredoxin metal center.[38]

was shown to react with the arylthiolate $\mathbf{L2}^-$ to provide $[Fe^{(III)}(\mathbf{L1})(\mathbf{L2})]^-$ in which $Fe^{(II)}$ is three-coordinate and weakly interacting with the benzylene bridge. As a matter of fact, it picks up a THF molecule reversibly, which, in association with the thiolate binding sites of $\mathbf{L1}^{2-}$ and $\mathbf{L2}^-$, complete the expected tetrahedral coordination sphere. Upon $2e^-$ reduction of $[Fe^{(III)}(\mathbf{L1})(\mathbf{L2})(THF)]^-$ by KC_8 under a dinitrogen atmosphere at low temperature, $\mathbf{L2}^-$ is released and the Fe complex $[Fe^{(0)}(\mathbf{L1})(N_2)]^{2-}$, in which the Fe atom is η^2-coordinated to the *m*-phenylene bridge, is obtained. Such a reaction sequence is remarkable as far as it supports one of the hypotheses for the binding of dinitrogen to the FeMoco. In this model, reduction/protonation of the cofactor releases one of the bridging sulfide as a monodentate hydrosulfide, which is followed by apical N_2 binding and Fe binding to the central carbide atom. Later, these authors showed that the $2e^-$ reduction of either $[Fe(\mathbf{L1})(\mathbf{L2})]^-$ or $[Fe^{(III)}(\mathbf{L1})(THF)_2]$ at low temperature afforded $[Fe^{(0)}(\mathbf{L1})]^{2-}$, in which the Fe atom is η^2-coordinated to the *m*-phenylene bridge.[40] This complex further reacted with dinitrogen to afford $[Fe^{(0)}(\mathbf{L1})(N_2)]^{2-}$.

2.3. Small tripod tri-thiolate ligands

Koch and coworkers synthesized the *o*-thiophenol analogue of tribenzylamine ($\mathbf{L3}H_3$), and showed that $\mathbf{L3}^{3-}$ could encapsulate an Fe^{2+} cation in a distorted tetrahedral environment, the distance between the plane of the three sulfur atoms and Fe^{2+} being 0.51 Å (Figure 5).[41]

Later on, they prepared the triphenyl-substituted phosphine $\mathbf{L4}H_3$.[42] They made the anionic $Ni^{(II)}$ and $Fe^{(II)}$ complexes of $\mathbf{L4}^{3-}$, and showed that the metal cations in these complexes could pick up a molecule of carbon monoxide, which was bound in the apical position, *trans* to the bridgehead phosphorus atom, the resulting pentacoordinate metal cation having the trigonal bipyramidal geometry. The authors noted that the coordination of CO in the axial position in the complex could be the result of the structural constraint exerted by the tripod ligand. In a related work,[43] they showed that the $Fe^{(II)}$ complex of the unsubstituted analogue $\mathbf{L5}H_3$ of $\mathbf{L4}H_3$ could pick up either CO

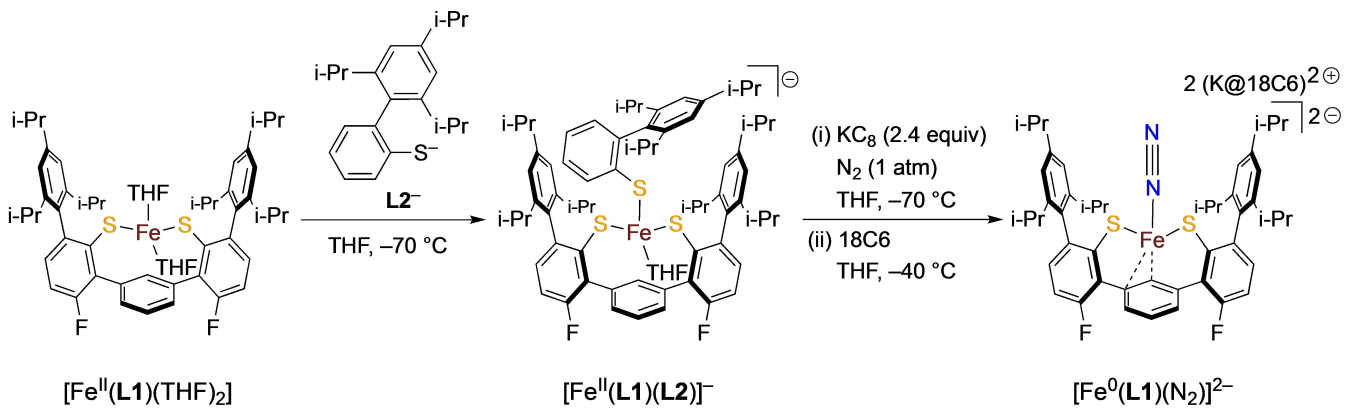

Figure 4. Sequence of reactions starting from a $Fe^{(II)}$ complex with a bi(arylthiolate) chelate leading to an $Fe^{(0)}$ dinitrogen complex in which the iron is η^2-coordinated to the *m*-phenylene bridge.[39]

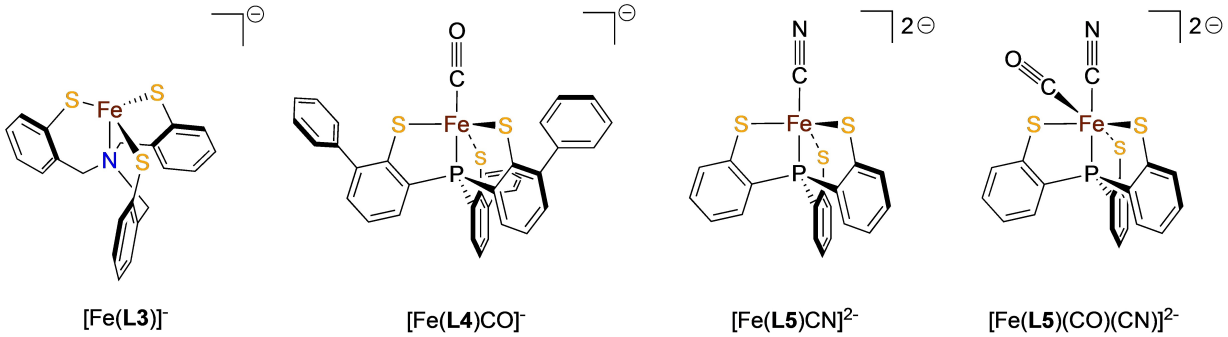

Figure 5. Examples of iron complexes of tripod tri(arylthiolate) ligands in which the metal cation is coordinated to the bridgehead N or P atom.[41–43]

or cyanide or both, and could be oxidized in both cases to the $Fe^{(III)}$ state. At that time, these compounds were the first examples of $Fe^{(II)}$ thiolate complexes with CN^- and CO, and their relevance to the mimicking of [NiFe] hydrogenases was mentioned.

The $V^{(III)}$ complex $[V(PC_6H_3\text{-}3\text{-}Me_3Si\text{-}2\text{-}S)_3Cl]^-$ **10** (Figure 6) was shown to catalyse the reduction of hydrazine to ammonia in acetonitrile in the form of the $V^{(II)}$ active species $[V(PC_6H_3\text{-}3\text{-}Me_3Si\text{-}2\text{-}S)_3(CH_3CN)]^-$ **11**, obtained by one e^- reduction by $[Co(Cp)_2]$, and in the presence of a source of protons (2,6-lutidinium chloride).[44] A maximum of 5 equivalents of hydrazine could be reduced nearly quantitatively, a larger excess of hydrazine saturating the coordination sphere of $V^{(II)}$. It must be noted that the use of a complex lacking the TMS substituents *ortho* to the thiolate did not perform this reduction, because the $V^{(III)}/V^{(II)}$ redox potential in this complex was much lower than in the former. As a consequence, $V^{(III)}$ could not be reduced to $V^{(II)}$ by $[Co(Cp)_2]$. Similar observations were done upon using the $Fe^{(II)}$ complex $[Fe(PC_6H_3\text{-}3\text{-}Me_3Si\text{-}2\text{-}S)_3(CH_3CN)]^-$ **12**, for which the X-ray crystal structures of the hydrazine and ammonia adducts were obtained.[45]

2.4. Tripod ligands based on cysteinate binding units

Delangle and coworkers reported a series of tripod ligands **L6**–**L9** deriving from the nitrilotriacetic acid platform and three cysteine binding sites (Figure 7).[46] They showed, by EXAFS analyses, that only the ester and amide ligands **L6** and **L7** could stabilize mononuclear $Cu^{(I)}$ complexes in a C_3-symmetrical trigonal planar coordination geometry at low $Cu^{(I)}$ concentration, the corresponding log *K* being 19.2 and 18.8, respectively. Remarkably, the selectivity of $Cu^{(I)}$ vs. $Zn^{(II)}$ binding was large (8-9 orders of magnitude), which is quite interesting as $Zn^{(II)}$ is a strong competitor of $Cu^{(I)}$ in cells. In addition, these ligands better fitted the smaller size of $Cu^{(I)}$ by comparison with $Hg^{(II)}$. As shown by EXAFS experiments, the $[Hg^{(II)}\mathbf{L6}]^-$ and $[Hg^{(II)}\mathbf{L7}]^-$ complexes showed three different Hg–S distances, and therefore departed from the true C_3 symmetry of the $Cu^{(I)}$ complexes. At high $Cu^{(I)}$ concentration the mononuclear complex was in equilibrium with an aggregate of $(Cu_2\mathbf{L6})_3$ stoichiometry, and in the case of **L8** and **L9**, only $Cu^{(I)}$ aggregates could be detected. Again, EXAFS investigations were used to determine the interatomic Cu···Cu and Cu–S distances, which were shown to be similar to those found in copper proteins such as metallothioneins (MTs).

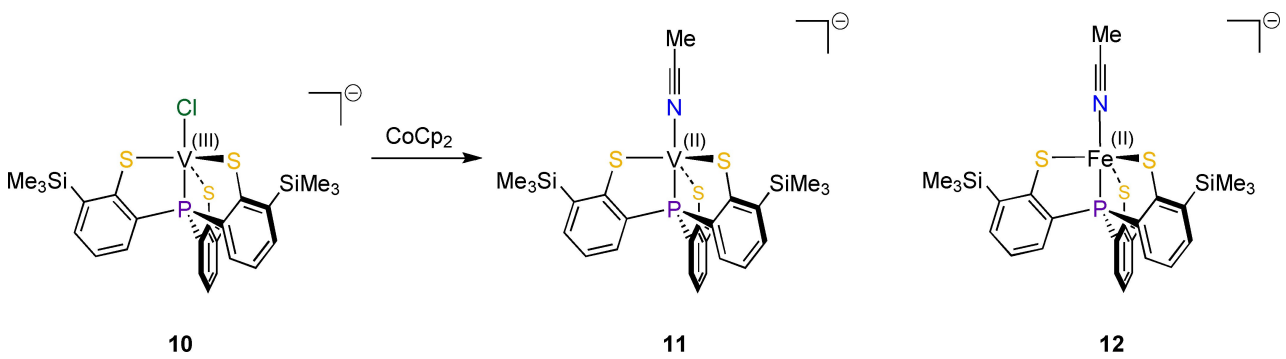

Figure 6. A $V^{(II)}$ and a $Fe^{(II)}$ complex with a tri(arylthiolate) tripod including a phosphorus bridgehead atom. The iron complex also binds a hydrazine molecule.[44,45]

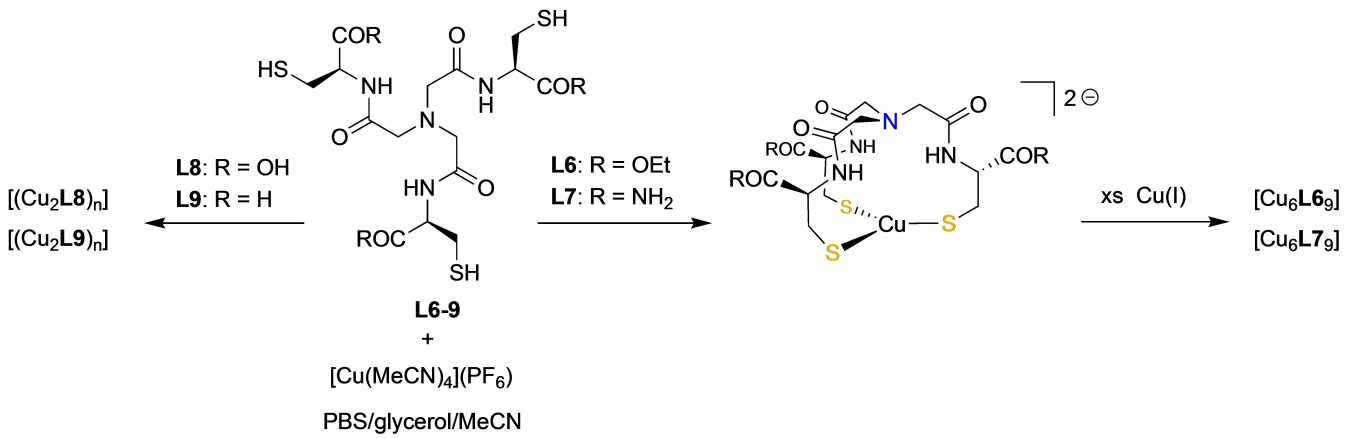

Figure 7. A $Cu^{(I)}$ complex with a tripod ligand incorporating cysteinate binding units.[46]

2.5. Sterically-hindered tripod ligands with thione donor atoms

Parkin and coworkers have introduced the thione analogue of the tris(3-*tert*-butylpyrazolylhydroborato) tripod ligand, which is obtained by deprotonation of the tris(2-mercapto-1-R-imidazolyl)hydroborato (**L10**^{R}) tripod. They have shown that this ligand was effective at stabilizing monomeric tetrahedral zinc complexes. They used it to study $Zn^{(II)}$ complexes in a sulfur-rich coordination environment in order to model the active sites of certain zinc enzymes (Figure 8).[47] For example, in 5-amino-levulinate dehydratase (ALAD), which catalyses the asymmetric dimerization of 5-aminolevulinic acid (ALA) to porphobilinogen, one of the Zn^{2+} ions of the active site is bound to three cysteinate and a water molecule.[47a] Therefore, the isolation of the complex [**L10**^{Ph}Zn(OH)] and the release of a water molecule in the presence of acid are quite significant in this respect. These authors also showed that **L10**^{Ph} could allow them to prepare tetrahedral $Zn^{(II)}$ complexes with four sulfur ligands, which mimicked the reactivity of the active site of the Ada DNA repair protein (a tetrahedral $[Zn(Cys)_4]$).[47b] Using *N*-phenyl-2-mercaptoacetamide as substrate and fourth ligand they prepared the complex [**L10**^{Ph}Zn($SCH_2C(O)NHPh$)] and showed that it readily reacted with an alkylating reagent (methyliodide) to release the thioether. Moreover, the X-ray crystal structure of the complex [**L10**^{Ph}Zn($SCH_2C(O)NHPh$)] gave evidence of an intramolecular NH···S^- hydrogen bond between the amide proton and the thiolate sulfur of the substrate. This observation is highly significant, because it has been postulated that NH···S^- hydrogen interactions provide a mechanism to modulate the reactivity of the zinc-cysteine thiolate moiety in the Ada DNA repair protein.

2.6. Complexation of Fe(II) in an octahedral geometry with nitrogenase substrates in a sulfur-rich environment

In a seminal work, Sellmann and coworkers designed a mixed thiolate/thioether/amine pentadentate ligand **L11**$^{2-}$, which provided $Fe^{(II)}$ with a square pyramidal geometry, the four sulfur atoms lying in the basal plane.[48] They could prepare the complex [Fe(**L11**)(NH_2NH_2)], in which the sixth coordination position was occupied by hydrazine, the product of the four-electron reduction of dinitrogen (Figure 9). This complex had an

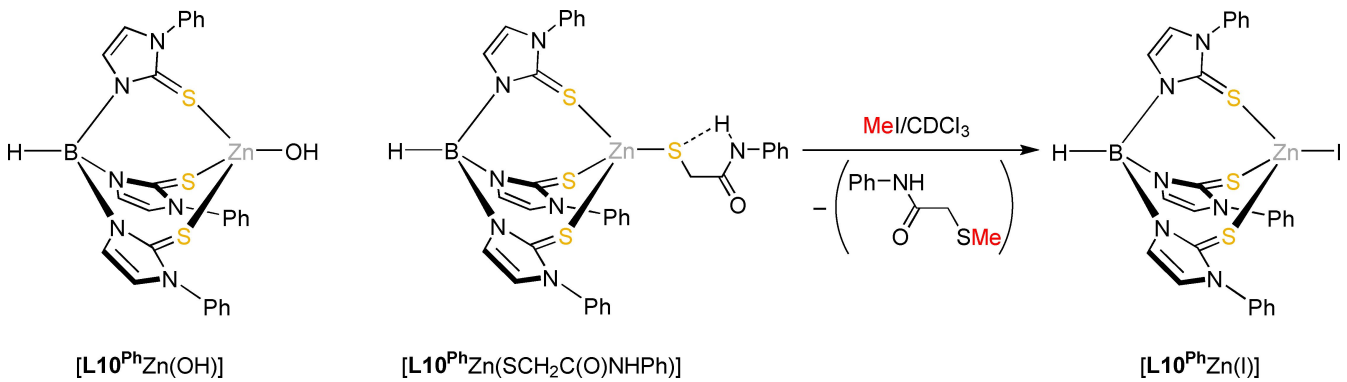

Figure 8. Tetrahedral $Zn^{(II)}$ complexes in a sulfur-rich environment mimicking the active sites of 5-aminolevulinate dehydratase ALAD ([**L10**^{Ph}Zn(OH)]) and Ada DNA ([**L10**^{Ph}Zn($SCH_2C(O)NHPh$)]).[47b]

Review
doi.org/10.1002/ejic.202200739

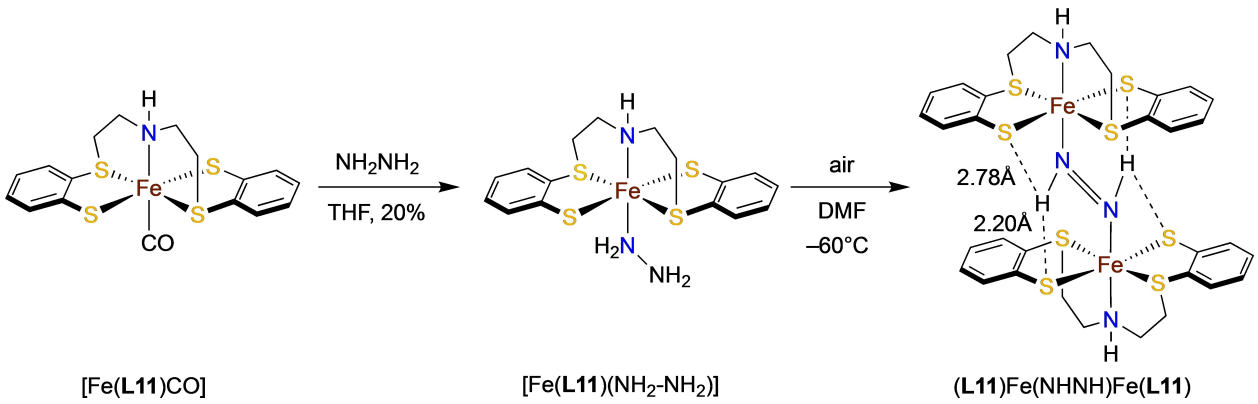

Figure 9. Complexation of hydrazine to $Fe^{(II)}$ in a sulfur-rich coordination environment and oxidation of bound hydrazine to diazene resulting in a diazene-bridged, dinuclear $Fe^{(II)}$ complex.[48]

unprecedented reactivity, which was not observed so far elsewhere: Its air oxidation let to the formation of the binuclear $Fe^{(II)}$ complex [(**L11**)Fe(NHNH)Fe(**L11**)] in which two Fe(**L11**) subunits are bridged by diazene, the product of the two-electron reduction/oxidation of dinitrogen/hydrazine. Interestingly, the X-ray crystal structure of [(**L11**)Fe(NHNH)Fe(**L11**)] showed bifurcated hydrogen bonds between the diazene protons and the bound thiolate sulfur atoms.

2.7. Tri-thiolate ligands from a protein

Pecoraro and coworkers have designed and synthesized α_3D**IV**, a single peptide chain deriving from the known α_3D, which is a de novo designed three-helix bundle protein.[49] α_3D**IV** differs from α_3D by the fact that three cysteines have been placed at chosen locations in each of the antiparallel three helix bundles.[50] The authors established first that α_3D**IV** was well-folded and stable in solution, then they titrated the protein with Hg^{2+}, Cd^{2+}, and Pb^{2+} ions. The binding constant of Hg^{2+} was too high to be measured, but those of Cd^{2+} and Pb^{2+} were determined to be 2.0×10^7 and $3.1\times10^7\ M^{-1}$, respectively. By comparing the pH dependence of the complexation of these metal cations to literature data, the authors deduced the nature and geometry of their coordination spheres: trigonal-planar for Hg^{2+}, pseudo-tetrahedral for Cd^{2+}, the fourth binding site being provided by a water molecule, and trigonal-pyramidal for Pb^{2+}. Although not noted by their authors, this work has a high significance as far as the peptide α_3D**IV** mimicks one of the functions of small proteins known as metallothioneins, that is, the sequestration of heavy metal cations such as Hg^{2+}, Cd^{2+}, and Pb^{2+} from living organisms and their components. In section 6a we shall see other examples of compounds behaving as metallothioneins, but, unlike the example shown here, without any relationships with biological compounds.

3. Complexation of Two Metal Cations by Thiolate Ligands: The Diamond $[M_2S_2]$ Motif

As outlined in the introduction, natural examples of binuclear complexes featuring two thiolate bridges and corresponding to the butterfly $[Fe_2S_2]$ core (in which S is an organic sulfur) are the [FeFe] and [NiFe] hydrogenases. The diamond $[M_2S_2]$ core is also found in the Cu_A center of cytochrome-c oxidase in which the copper cations are bridged by two cysteinate sulfur, the coordination sphere of each being completed by an imidazole nitrogen, another cysteinate sulfur for one and an aspartate oxygen for the other. In such coordination environments, the transfer of one electron from and to Cu_A is very fast and perfectly reversible.

3.1. 1,2-benzene dithiolate as bridging ligand for a functional model of the H active site of [FeFe] hydrogenase

Dithiolate ligands can not only play the role of chelates, but also of bridging ligands. As a matter of fact, 1,2-benzene dithiolate **bdt**$^{2-}$ has been used for mimicking the two bridging cysteine thiolates found in the butterfly $[Fe_2S_2]$ structure of the so-called H-cluster of [FeFe]-hydrogenases, in which the coordination sphere of the Fe^{n+} cations is completed by biologically relevant CO and CN^- ligands or artificial PR_3 and N-heterocyclic carbene (NHC) ligands.[51] In particular, the symmetrical $[(CO)_3Fe(\mathbf{bdt})Fe(CO)_3]$ complex has been shown to behave as an interesting catalyst for the proton reduction with low overpotentials and less negative potentials in reducing processes, but we focus on the complex [Cp*Fe(μ-η^2:η^4-**bdt**)FeCp*] (**13**, Figure 10), because it was shown to catalyse the conversion of diazene HN=NH to ammonia.[52] The fact that it can be also used as an electrocatalyst for H_2 production is highly significant, as nitrogenases also behave as hydrogenases.[20f] **13** was protonated by HBF_4 in CH_2Cl_2 ($-78\,^\circ C$ to r. t.), affording **14**(BF_4), in which a proton was shown to bridge the two metal cations. Then, one-electron reduction of **14**(BF_4) by $[Co(Cp)_2]$ afforded the mixed-valence $[Fe^{(II)}Fe^{(III)}]$ hydride complex **15**, which was

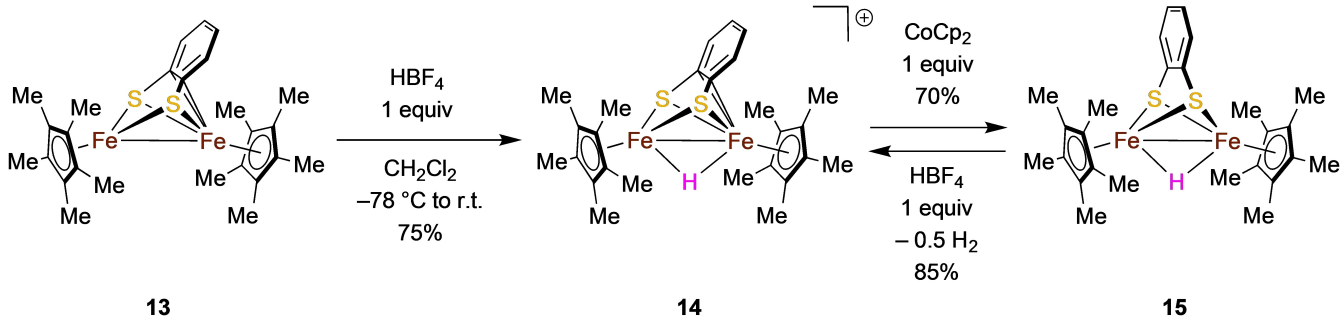

Figure 10. Sequential protonation and reduction of a binuclear $Fe^{(II)}$ complex with an Fe–Fe bond and a benzene dithiolate bridge led to a hydride complex which, after further protonation, evolved H_2.[52]

characterized, in particular, by single crystal X-ray crystallography. Variable temperature NMR experiments allowed the authors to identify an intermediate at low temperatures, in which the proton coordinated first a single Fe atom before bridging both at r. t. **14**(BF_4) was shown, by cyclic voltammetry, to behave as an electrocatalyst for dihydrogen production in the presence of controlled amounts of HBF_4.

3.2. Oxidation of dihydrogen catalysed by a dinuclear [RuRu] complex

The binuclear [$Ru^{(III)}Ru^{(III)}$] complex **16** (Figure 11) resembles the [$Fe^{(II)}Fe^{(II)}$] complex **13** of section 3a, except that the **bdt**$^{2-}$ ligand has been replaced by a triphenylphosphine analogue in which two of the Ph substituents of PPh_3 have been changed to an *o*-thiophenolate.[53] This ligand plays a double role: a terminal phosphine ligand for one of the ruthenium cations, and a double thiolate bridge for the two metals. The complex **16** was shown to be reduced by 1 atm of dihydrogen in water to the hydride complex **17**, in which the H^- ligand was bound to the low-coordinate ruthenium, with release of a stoichiometric amount of HOTf. In addition, **17** was shown to be oxidized back to **16** by [$Fe(Cp)_2$](OTf) in dichloromethane with evolution of half an equivalent of dihydrogen. Further, oxidation of dihydrogen in the presence of catalytic amounts of **16** and stoichiometric amounts of P(*o*-Tol)$_3$ as base and [$Fe(Cp)_2$](OTf) as oxidant in CH_2Cl_2 with a TON as high as 9900 was observed. In agreement with the preliminary experiments, the catalysis could also be run in water (which played the role of the base) but gave a lower TON (*ca* 100). Therefore, **16** worked as an efficient organometallic anode catalyst for the fuel cell.

3.3. A structural and functional model of the biological Cu_A site

Duboc and coworkers designed a 2,2′-bipyridine ligand **L12**$^{2-}$ bearing thioethylene substituents in which methyl groups attached to the *CS*$^-$ carbon atom helped to control the environment and reactivity of the thiolate.[54] They showed that, in the presence of CuCl, **L12**$^{2-}$ formed an unsymmetrical (with respect to the 2,2′-bipyridine core) dinuclear complex [Cu_2(**L12**)$_2$] in which one thiolate sulfur atom of each **L12**$^{2-}$ played the role of a bridge between the Cu^+ cations, while the remaining two sulfur atoms are engaged in a 1,2-dithiane fragment (Figure 12). This bis(μ-thiolato) dicopper complex was shown to mimic the key structural and spectroscopic features of Cu_A (e.g., short Cu···Cu distance of 2.64 Å in the reduced, [$Cu^{(I)}Cu^{(I)}$] state) and its redox reactivity, leading to the delocalized mixed-valence state upon one-electron oxidation, the process being perfectly reversible.

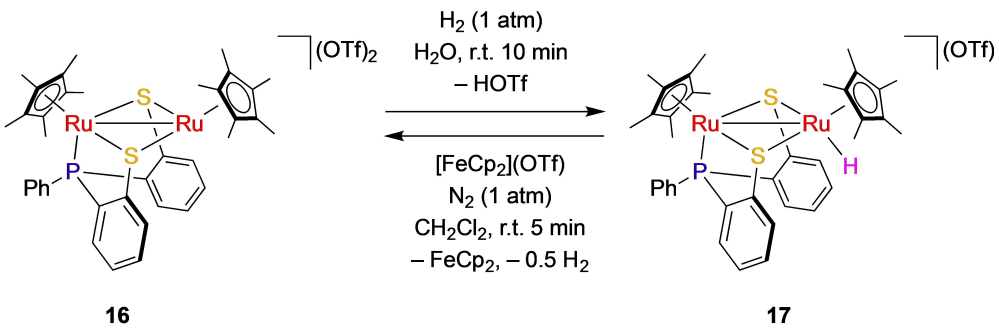

Figure 11. A binuclear $Ru^{(III)}$ dication exhibiting similar characteristics as complex **13**, reacted with H_2 to form a hydride complex, which could be oxidized back to the starting complex in the presence of HOTf.[53]

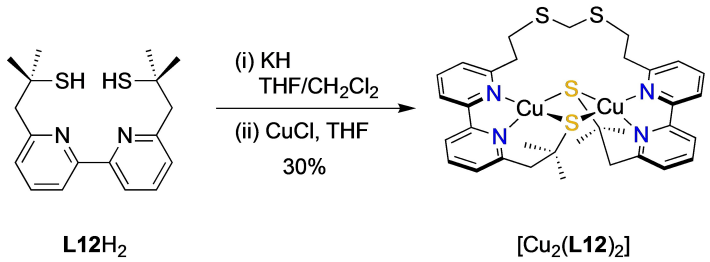

Figure 12. Dimerization of a bipyridine ligand incorporating two thiolate arms in the presence of $Cu^{(I)}$ and methylene chloride.[54]

3.4. Complexation of two metal cations by a small tri-thiolate tripod

The tri-thiolate tripod **L13**H_3 based on the TACN macrocycle was designed by Wieghardt and coworkers (Figure 13).[55] The three secondary amine nitrogen atoms of TACN and the three aryl thiolate pendent arms can provide an octahedral [N3S3] coordination geometry to a range of trivalent metal cations ($Ga^{(III)}$, $In^{(III)}$, $V^{(III)}$, $Cr^{(III)}$, $Mn^{(III)}$, $Fe^{(III)}$, $Co^{(III)}$), as well to the oxidized $V^{(IV)}$ and $Mn^{(IV)}$. Interestingly, the reaction of **L13**H_3·3HCl with divalent metal chlorides MCl_2·$6H_2O$ (M=$Mn^{(II)}$, $Co^{(II)}$, $Ni^{(II)}$, $Zn^{(II)}$, and $Cd^{(II)}$) in anaerobic conditions directly afforded the homo-dinuclear complexes [**L13** M_2Cl] in which one metal cation is six-coordinate whereas the second metal cation is four-coordinate in a tetrahedral [S3Cl] coordination geometry. Heterodinuclear complexes [**L13** M^1M^2Cl] (M^1 = Zn, M^2 = Fe, Co, and Ni; M^1 = Ni; M^2 = Co and Zn; M^1 = Mn; M^2 = Fe, Co, Ni, Zn, Cd, and Hg) were prepared by reaction of [**L13** M^1]$^-$ (obtained either in situ from [**L13** M^1M^1Cl] by abstraction of the outer M^1 with tacn or by 1:1 reaction mixture of **L13**H_3 and M^1) and M^2Cl_2·$6H_2O$ in the presence of Et_4NCl.

4. Compartmental Nitrogen-based Macrocycles Incorporating Thiolate Donors

Compartmental macrocycles that use nitrogen and sulfur functionalities as donors for coordinating metal centers are suitable for the preparation of homo- and heteronuclear

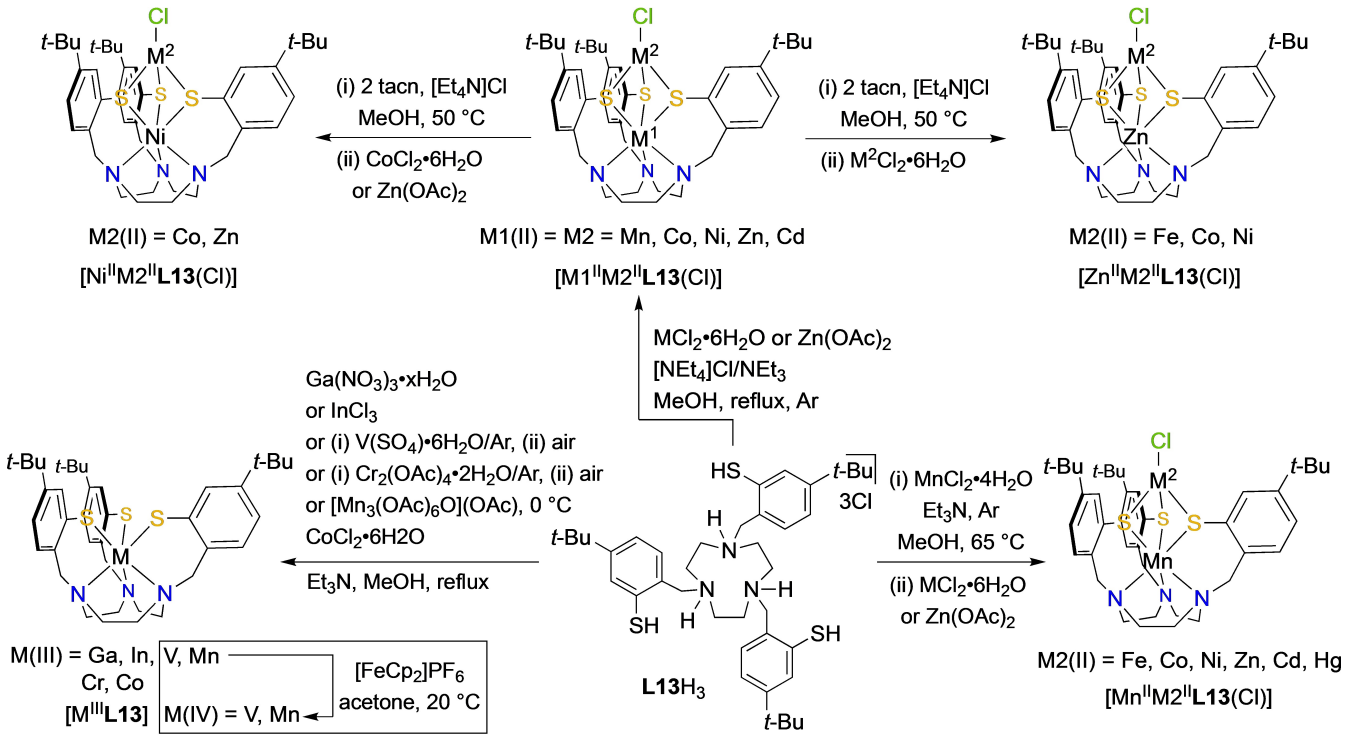

Figure 13. A tri(arylthiolate) tripod ligand based on the TACN macrocycle (**L13**$^{3-}$) showed a rich coordination chemistry with divalent, trivalent, and a few tetravalent metal cations. It could encapsulate a single metal cation in a [N3S3] coordination environment, or form homo- and hetero-dinuclear complexes in which the encapsulated and the exo metal cations were bridged by three arylthiolate subunits.[55]

complexes. As mentioned in the introduction these ligands are especially suited to model polymetallic metalloproteins in which metals in close proximity are bound to histidine and cysteine amino acid residues, by mimicking, in particular, the magnetic and electronic interactions between the coordinated metal centers. Therefore, compartmental nitrogen-based macrocyclic ligands incorporating thiolate bridges are of great interest and will be further described in detail in this section.[55–58]

4.1. Schiff-base macrocycles

First mentioned by Robson et al.,[59] Schiff-base macrocyclic complexes have been investigated ever since. The use of nitrogen-based macrocycles for the purpose to bind metals in close proximity has been reviewed by Brooker,[8] whose research group developed a wide range of Schiff-base ligands, including thiolate head units. Brooker used this technique to obtain Schiff-base macrocyclic dinuclear complexes such as **18** in Figure 14.

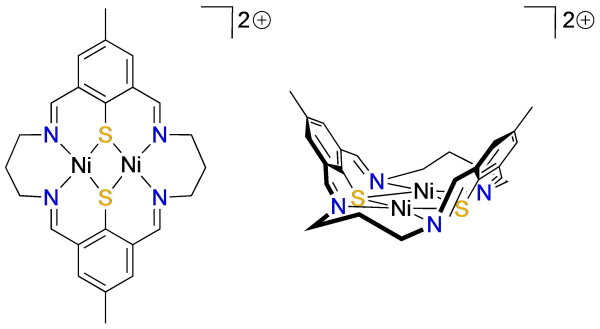

18

Figure 14. Two- (left) and three-dimensional (right) visualization of an imine-thiophenolate macrocycle forcing Ni^{2+} ions into a square planar coordination geometry.[8]

Schröder and co-workers reported biomimetic model compounds for NiFe hydrogenase, cytochrome c oxidase, and N_2O reductase utilising compartmental Schiff-base macrocycles.[56–58] Brooker et al. showed that phenolate and thiophenolate-incorporating ligands led to different metal coordination environments.[60] The thiophenolate compound offered the Ni^{2+} ions a square planar geometry, a low spin configuration and the distance between the Ni^{2+} centers was as short as 3.151(2) Å. Complex **18** exhibited a rich redox chemistry with four reversible one-electron redox processes: two reduction and two oxidation steps. Interestingly, the mixed valent $Ni^{(II)}Ni^{(III)}$ thiophenolate complex was isolated, however it was unstable even in the solid state.[8,60] In addition, the $Ni^{(II)}Ni^{(III)}$ system was sensitive to axial coordination by solvent molecules, as would be expected for a d^7 configurated $Ni^{(III)}$. These Schiff-base thiophenolate macrocycles turned out to be the ideal precursors for the development of the corresponding amine derivatives and their complexes, as shown in the following section.

4.2. Compartmental amine-thiophenolate macrocycles

Kersting and coworkers designed a compartmental ligand H_2**L14**^{R} that integrated two [N3S2] donor sets sharing the central thiolate donors to coordinate different metal centers.[61] First, two Ni^{2+} ions were implemented in the deprotonated macrocycle (**L14**^{Me})$^{2-}$ and (**L14**^{H})$^{2-}$ (Figure 15). The resulting complex exhibited two one-electron oxidations, although all $Ni^{(III)}Ni^{(III)}$ species of (**L14**^{R})$^{2-}$ were not stable on the timescale of a cyclic voltammetry experiment. This was in marked contrast to the behaviour of previously obtained coordinatively saturated Ni aminothiolate complexes, which could be reversibly oxidized to $Ni^{(III)}Ni^{(III)}$ species.[62]

The ligand **L14**^{R} was shown to be able to bind many transition metals in different redox states and electronic characteristics. Depending on the nature of the coligand L' and the coordinated metal centers the macrocyclic ligand shows two different conformations *A* and *B* (Figure 15b and c), which

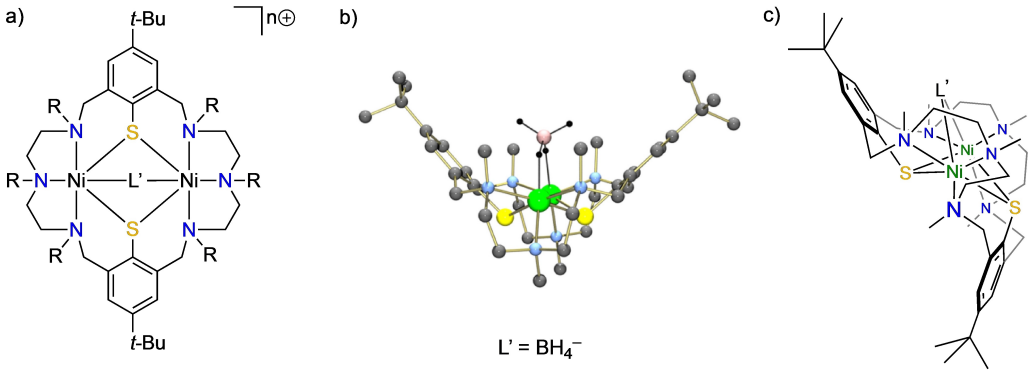

[Ni$_2$(**L14**^{R})L'] [Ni$_2$(**L14**^{Me})L'] (conf. *A*) [Ni$_2$(**L14**^{Me})L'] (conf. *B*)

Figure 15. a) Composition of mixed-ligand nickel complexes supported by the [N6S2] macrocycle **L14**^{R} (R=H or CH_3, L'=coligand; b) View of the molecular structure of the borohydrido-bridged Ni complex [Ni_2(**L**^{14Me})($\mu_{1,3}$-BH_4)]$^{-}$, which shows configuration *A* in the crystal.[63c] Hydrogen atoms omitted except those for the BH_4^- coligand. Color code: B pink, C grey, H black, N dark turquoise, Ni green, S yellow; c) general chemical structure of configuration *B*.[63a] Reproduced from Ref. [63c] with permission from the Royal Society of Chemistry.

Review
doi.org/10.1002/ejic.202200739

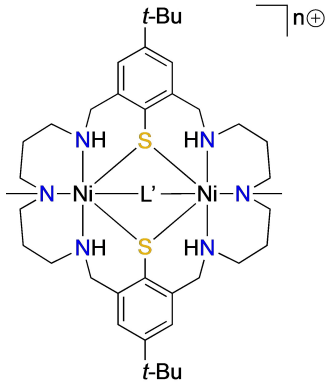

$[Ni_2(\mathbf{L15^{Me2H4}})L']^{n+}$

Figure 16. Structure of the complex derivative $[Ni_2(\mathbf{L15^{Me2H4}})L']^{n+}$ of $[Ni_2(\mathbf{L14^{R}})L']^{+}$ investigated for halide and pseudohalide recognition.[68]

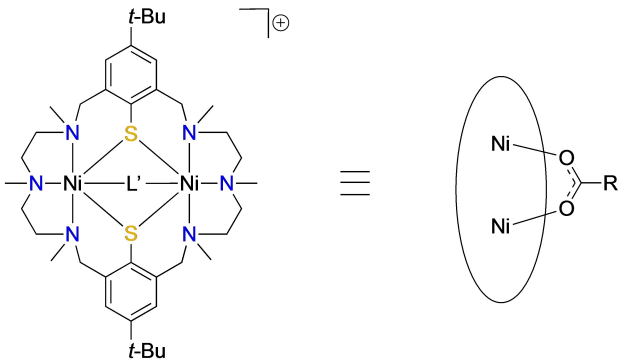

$[Ni_2\mathbf{L14^{Me}}CO_2R]^{+}$

Figure 17. Left: General structure of $\mu_{1,3}$-carboxylato-bridged complexes $[Ni_2(\mathbf{L14^{Me}})(\mu_{1,3}\text{-}CO_2R)]^{+}$. Right: Scheme of the binding mode of the carboxylate ligands $[Ni_2(\mathbf{L14^{Me}})(\mu_{1,3}\text{-}CO_2R)]^{+}$. The macrocyclic supporting ligand is represented by the ellipse.[69]

are comparable to the cone (*A*) and partial cone (*B*) conformations of the calixarenes. The following binuclear complexes of this macrocycle have been prepared: Ni^{2+}, Zn^{2+}, Cd^{2+}, Zn^{2+}/Cd^{2+}, Co^{2+}, Co^{3+}, $Co^{2+/3+}$, Mn^{2+}, Fe^{2+}, Cr^{3+}, Hg^{2+}, Cd^{2+}, Pb^{2+}.[26] Except the latter three, all the mentioned cations feature a bi-octahedral $N_3M(\mu\text{-}S)_2(\mu\text{-}L')MN_3$ metal core structure, irrespective of the type of the coligand L′ or the substitution **R** of the supporting macrocycle $\mathbf{L14^{R}}$. The divalent and trivalent metal ions are coordinated in a square-pyramidal fashion by the two *fac*-$N_3(\mu\text{-}S)_2$ donor sets of the macrocycles. Upon coordination of the exogenous coligands **L′14** distorted octahedral environments result for the metal atoms. The M···M distances vary from 3.037 to 3.527 Å.[63]

A detailed comparison of the individual structures showed that the conformation of the amino-thiophenolates was coupled to the size of the coligand L′ and the metal ion radii. For the complexes of the 3d elements the type *B* conformation was observed only for small monoatomic bridging ligands such as OH^- and Cl^-. For large monoatomic coligands L′ (such as SH^-) or a multiatom bridging ligand (such as OAc^-) the bowl-shaped conformation *A* was observed, the driving force, in both cases, being the more regular octahedral coordination environment about the M^{2+} ions.

4.3. Metal-metal interactions in dinuclear complexes supported by compartmental amino-thiophenolate macrocycles

An analysis of the magnetic susceptibility data for the $Ni^{2+}Ni^{2+}$ complex of $\mathbf{L14^{Me}}$ with a hypophosphito ($H_2PO_2^-$) bridge as co-ligand revealed the occurrence of ferromagnetic exchange interactions between the Ni^{2+} ($S=1$) ions with a value for the magnetic exchange coupling constant J of $+22\ cm^{-1}$ ($H=-2JS_1S_2$).[64] The complex $[Ni_2(\mathbf{L14^{Me}})(H_2PO_2)]^{+}$ has a remarkably high stability against reduction whatever the temperature and the nature of the solvent. Other $Ni^{(II)}$ complexes with hypophosphite are readily reduced to elemental nickel.[65] The reluctance can be attributed to encapsulation in a molecular pocket, which has precedence in the literature.[66]

Other investigations of the metal-metal interactions were carried out with the $Co^{(II)/(III)}$ and the $Cr^{(III)}$ complexes of $\mathbf{L14^{Me}}$. The redox chemistry of the $Co^{(II)/(III)}$, $Ni^{(II)}$ and $Cr^{(III)}$ complexes was investigated for many coligands L′ by cyclic voltammetry, which showed one electron oxidation and reduction processes. The redox chemistry was investigated for $[Co^{(II)}{}_2(\mathbf{L14^{Me}})(Cl)]^{+}$ and three of its derivatives (L′ = μ-O_2CMe, μ-O_2CCH=CHPh, and μ-O_2COMe). These complexes exhibited two reversible one-

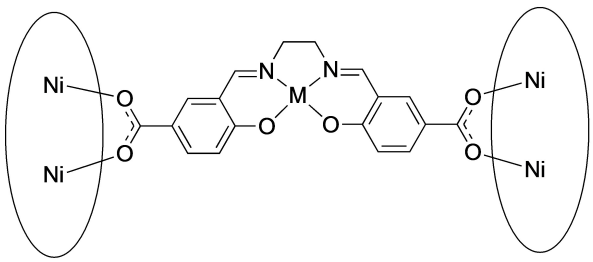

19

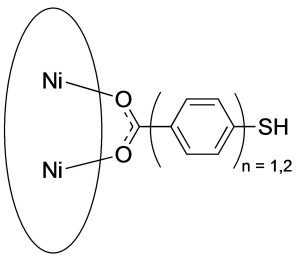

20

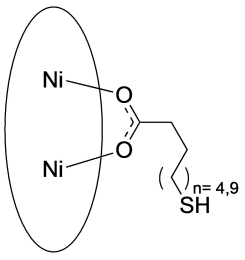

21

Figure 18. (Left) Bis-$[Ni_2(\mathbf{L14^{Me}})]$ complex **19** with the bridging [(μ-salen)M] coligand: M=$Ni^{(II)}$, $Cu^{(II)}$, $Pd^{(II)}$. (Right) $[Ni_2(\mathbf{L14^{Me}})L']^{+}$ complexes **20** and **21** with L′ = ω-mercapto-carboxylato coligand with the linear configuration of the aryl bridge and the bent configuration of the alkyl bridge.[70,71]

Review
doi.org/10.1002/ejic.202200739

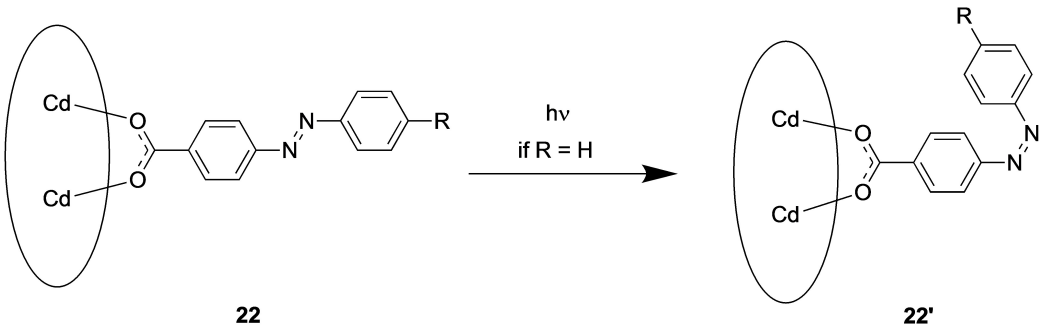

Figure 19. $[Cd_2(\mathbf{L14^{Me}})L']^+$ with an azobenzene-carboxylato coligand. For R=H the complex shows two photoswitchable configurations **22** and **22'**.[72]

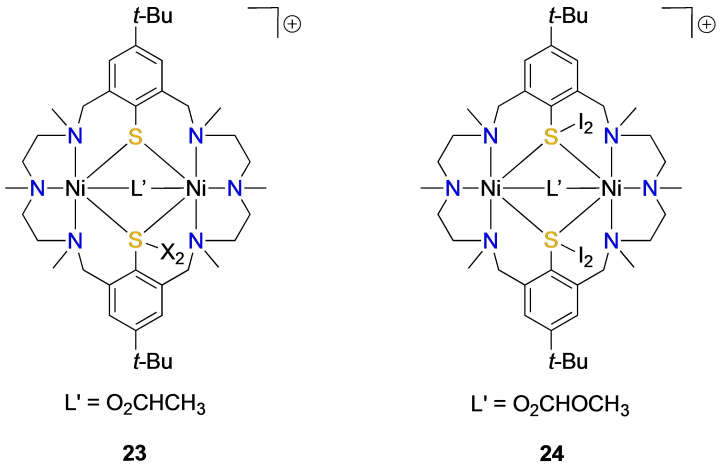

Figure 20. Structures of charge transfer adducts **23** and **24** formed between the thiolate complexes $[Ni_2(\mathbf{L14^{Me}})O_2CCH_3]^+$ and $[Ni_2(\mathbf{L14^{Me}})O_2COCH_3]^+$ with halogen molecules (X_2 = Br_2, I_2). The RS→X–X linkages in **23** and **24** adopt a linear geometry.[73]

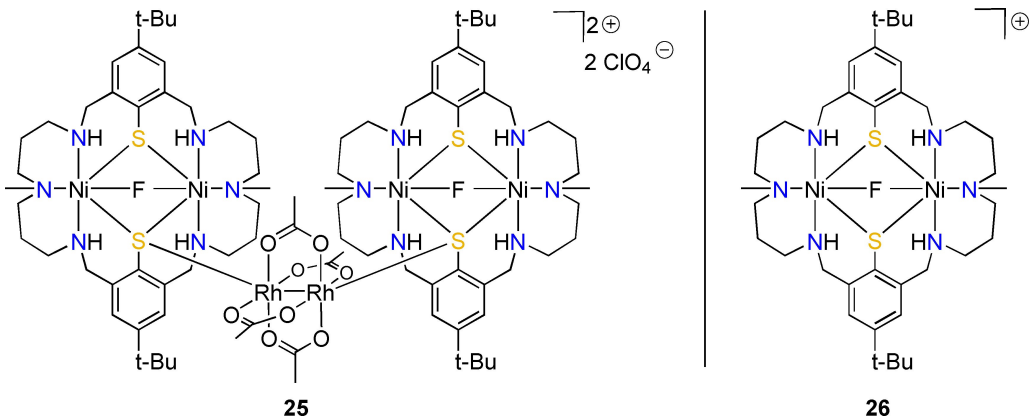

Figure 21. $[M^{(II)}{}_2(\mathbf{L15^{Me2H4}})(F)]$ CT-complexes with different metal complex subunits. Left: Bridging of two $[Ni^{(II)}{}_2(\mathbf{L15^{Me2H4}})(F)]^-$ complex subunits by $Rh_2(OAc)_4$ to form **25**. Right: 1:1 CT complex **26** between $[\{M^{(II)}{}_2(\mathbf{L15^{Me2H4}})(F_2)\}]^-$, M=$Co^{(II)}$ or $Ni^{(II)}$ and $[Cu^{(I)}(X_2)]$, X=Cl, Br, and I.[75]

electron oxidation processes; namely $Co^{(III)}Co^{(II)}/Co^{(II)}Co^{(II)}$ and $Co^{(III)}Co^{(III)}/Co^{(III)}Co^{(II)}$. The oxidized species were obtained by chemical oxidation by using mild oxidizing agents (I_2 to obtain the mixed valent $[Co^{(II)}Co^{(III)}]^{2+}$ dications and Br_2 to obtain the fully oxidized $[Co^{(III)}{}_2]^{3+}$ trication). They were isolated and investigated by X-ray diffraction. The corresponding Co–Co bond lengths differ only slightly, but the individual Co–N and Co–S bond lengths vary widely. The observed differences in the individual Co–N and Co–S distances could be attributed to steric constraints of the macrocyclic ligand, rather than to a specific metal d^n electronic configuration. Finally, the C–O bond lengths are identical within experimental error; they are typical

Review
doi.org/10.1002/ejic.202200739

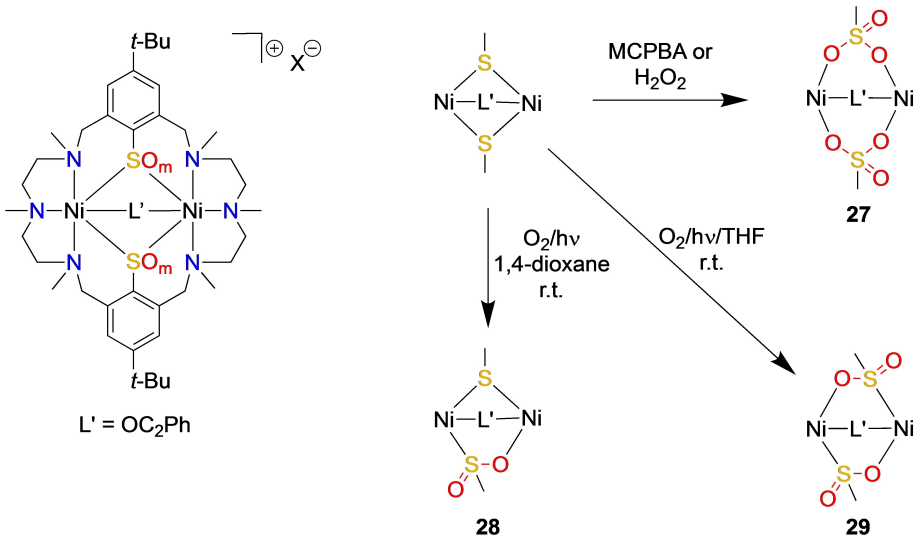

Figure 22. S-oxygenation reactions of the [N6S2]-$Ni^{(II)}$ complex and core structures of the products from these reactions. L′ = OC_2Ph.[76]

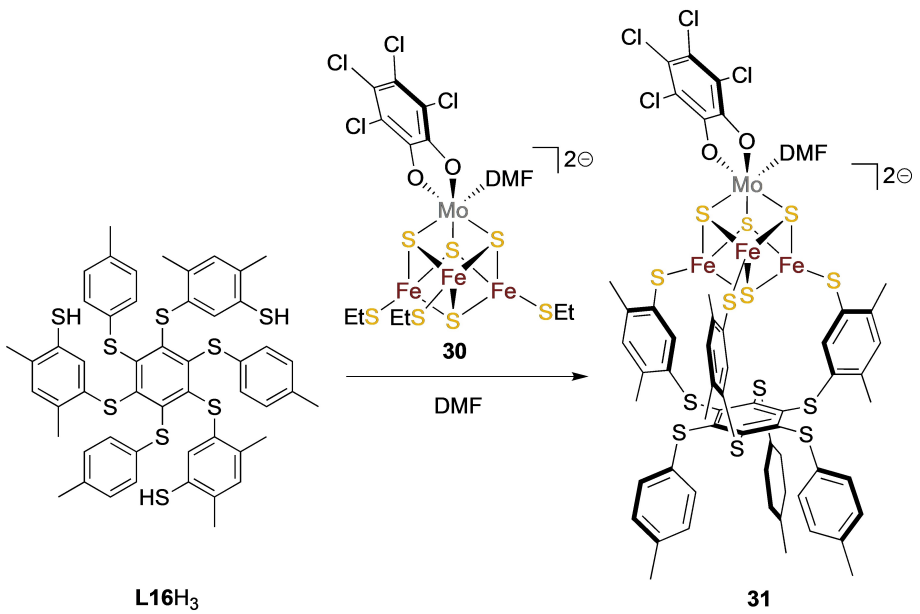

Figure 23. Complexation of an [$MoFe_3S_4$] heterocubane through a thiol/thiolate exchange reaction to give the assembly **31** by a highly preorganized tri-thiolate ligand (**L16**$^{3-}$) constructed on a hexathiabenzene platform.[77]

for bridging acetate groups.[67] Interestingly, all of the mixed-valent $Co^{(II)}/Co^{(III)}$ complexes showed localized high-spin $Co^{(II)}$ (d^7) and low-spin $Co^{(III)}$ (d^6) ions. These redox processes did not change the bowl-shaped structure of the complexes and the coligands remained in their bridging position.[68]

The air-stable $[Cr^{(III)}_2(\mathbf{L14^{Me}})L']^{3+}$ complexes required quite a low potential to be reduced to the divalent state, as $E^{0\prime}{}_{1/2}(Cr^{(III)}$-$Cr^{(II)}/Cr^{(II)}Cr^{(II)}) = -1.40$ V, whereas $E^{0\prime}{}_{1/2}(Cr^{(III)}Cr^{(III)}/Cr^{(III)}Cr^{(II)}) = -0.85$ V vs. $Fe(Cp)_2{}^+/Fe(Cp)_2$ for **L′14** being a carboxylate (formiate and benzoate). The $[Cr^{(III)}_2(\mathbf{L14^{Me}})(O_2CR)]^{3+}$ complexes exhibited ferromagnetic coupling between the $Cr^{(III)}$ centers. Here the magnitude of the coupling was three times higher than in other dinuclear $Cr^{(III)}$ complexes ($J = +24.2(2)$ cm^{-1} for the complex with formiate coligand and $J = +34.8(4)$ cm^{-1} for the complex with benzoate coligand).[63b]

4.4. Coligand binding and modification of the amine-based thiophenolate macrocyclic complexes

The reactivity of the dinuclear $[Ni^{II}_2(\mathbf{L14^{Me}})L']^{n+}$ complexes was examined in detail. These reactions included exchange of the coligands L′ of Figure 15 and S-oxygenation of the thiolate

Review
doi.org/10.1002/ejic.202200739

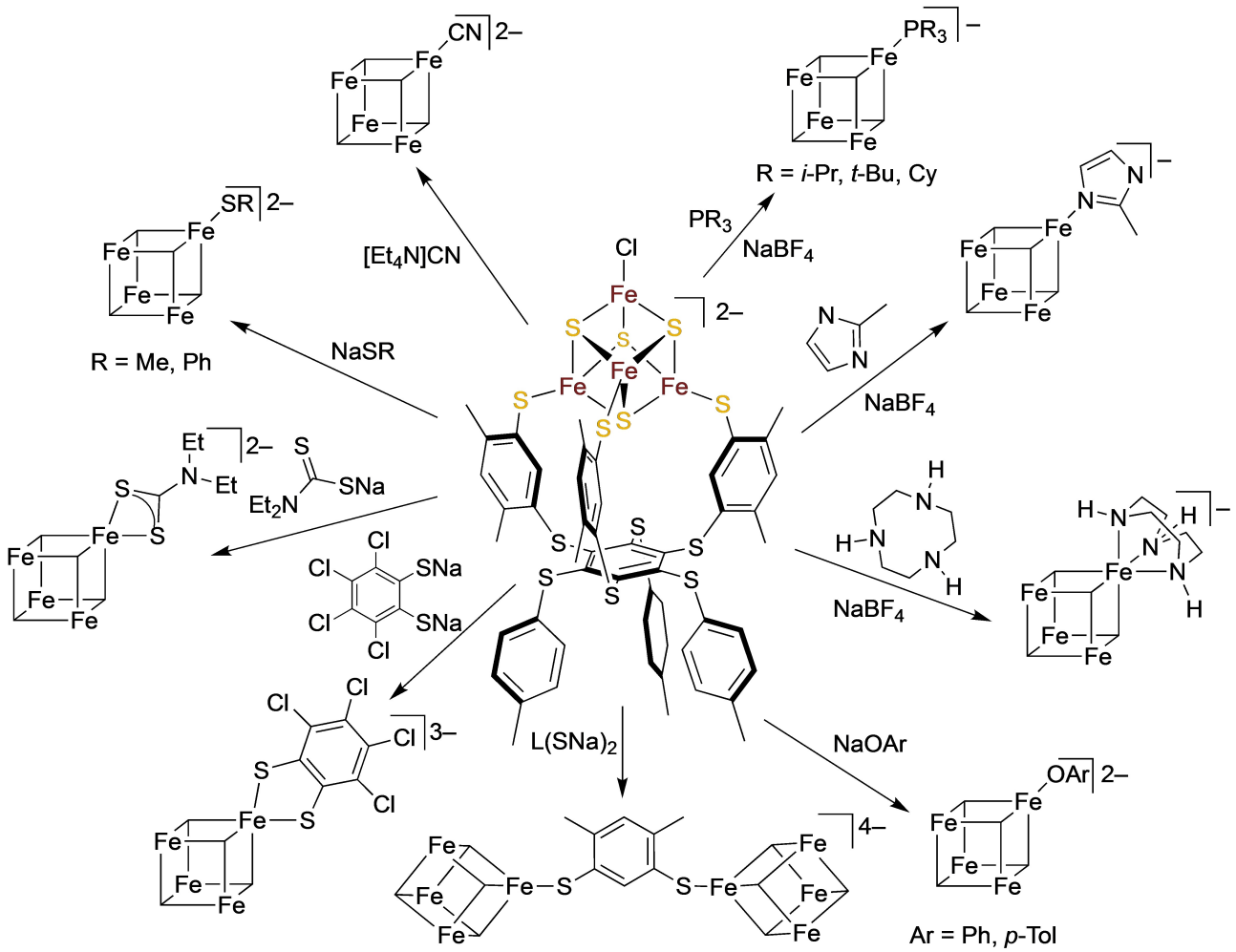

Figure 24. Illustration of the subsite-specific reactivity of an $[Fe_4S_4]^{2-}$ cluster made possible by the use of the tri(arylthiolate) ligand **L16**$^{3-}$, which literally grabbed the cluster by three of the four iron cations, leaving one complexed with an auxiliary ligand (here Cl^-), which could be exchanged for a large variety of mono-, bi-, and even tridentate ligands. Note that the S^{2-} bridging anions of the $[Fe_4S_4]^{2-}$ cluster subunits are not shown for clarity.[77]

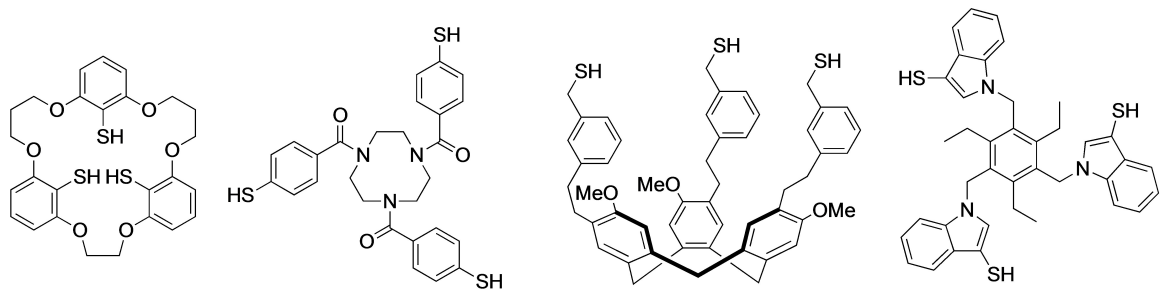

32 **33** **34** **35**

Figure 25. Examples of the tri(arylthiols) (**32**–**35**) that were shown to be able, after thiol deprotonation, to bind $[Fe_4S_4]^{2-}$ clusters.[78–82]

functionalities of the supporting ligand, respectively. Selected reactions are described in this section.

4.4.1. Anion recognition by amine-based thiophenolate macrocyclic complexes

The binding of various anions by the coordinatively unsaturated complex $[Ni^{(II)}_2(\mathbf{L15^{Me2H4}})]^+$ (Figure 16) was examined by spectrophotometric titration and isothermal titration calorimetry in

Review
doi.org/10.1002/ejic.202200739

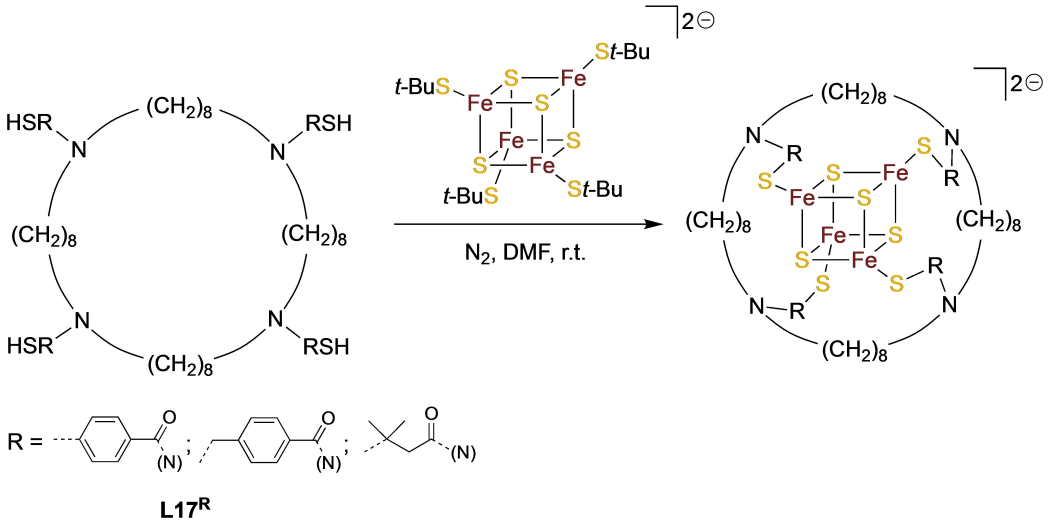

Figure 26. Encapsulation of an $[Fe_4S_4]^{2-}$ cubane by the macrocycles $(\mathbf{L17^R})^{4-}$ appended with four thiolate arms.[83]

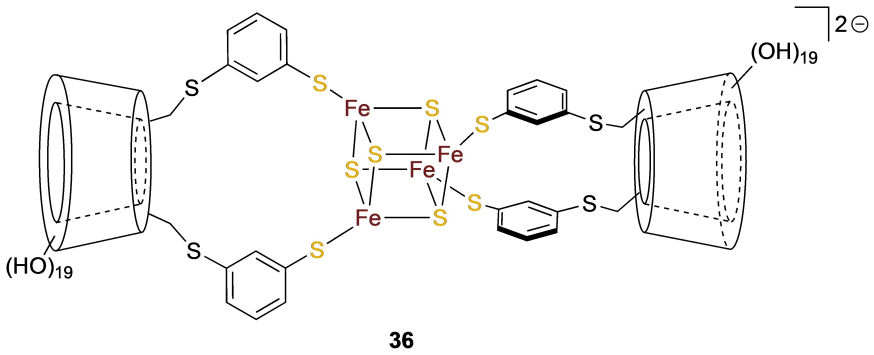

Figure 27. Encapsulation of a $[Fe_4S_4]$ cluster by two β-cyclodextrins bearing two thiophenolate groups that are anchored at the A, D positions of the small rim to give the assembly **36**.[84]

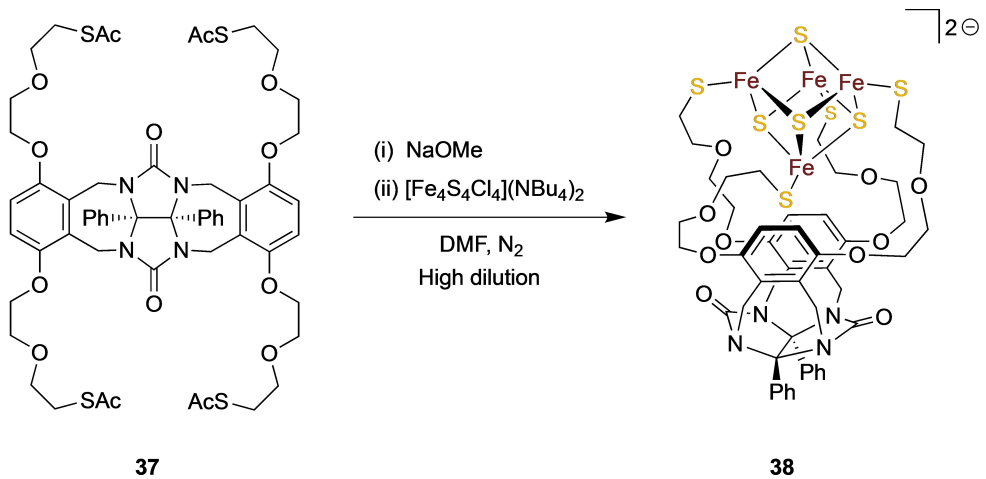

Figure 28. Encapsulation of a $[Fe_4S_4]$ cluster in assembly **38** by a glycoluril-based molecular platform substituted by four remote thiolate functions after deacetylation of precursor **37**.[85]

solution. This complex reacts with fluoride, chloride, bromide and hydroxide ions to afford an isostructural series of halogen-ido- or hydroxide-bridged complexes $[Ni_2(\mathbf{L15^{Me2H4}})(\mu\text{-}L')]^+$ featuring a N3Ni(μ-S)$_2$(μ-L′)NiN3 core structure. No reactions

Review
doi.org/10.1002/ejic.202200739

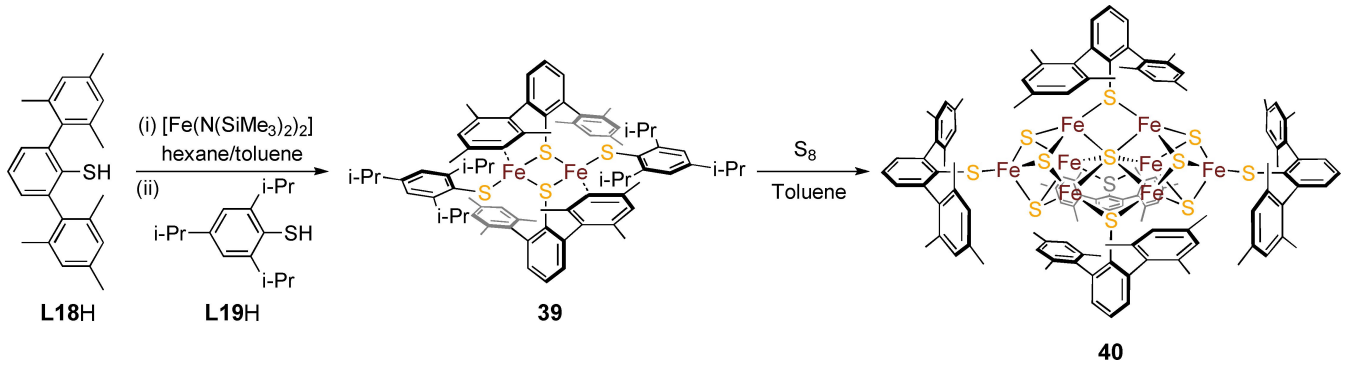

Figure 29. Preparation of the $[Fe_8S_7(SAr)_5]$ cluster **40** by reaction of the dinuclear iron-sulfur complex **39** with elemental sulfur.[86]

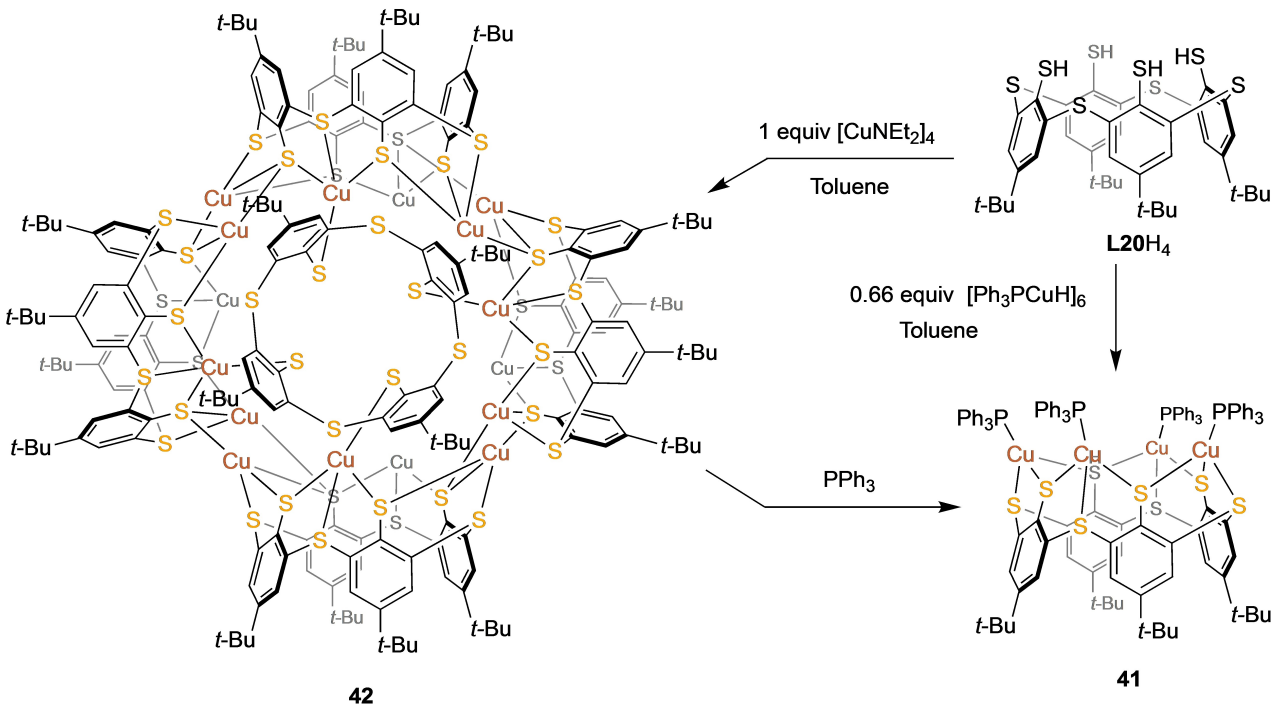

Figure 30. Reaction of tetrathiatetramercaptocalix[4]arene with the $Cu^{(I)}$ tetramer $[CuNEt_2]_4$ leads to a sphere-like complex $(Cu_4\mathbf{L20})_6$ (**42**) of Cu/**L20** 24:6 composition in which the 24 Cu^+ cations are each complexed by three arylthiolate sulfur anions and one diarylthioether sulfur atom. The giant calix[4]arene hexamer can be broken to a monomer by reaction with PPh_3. 8 Cu^+ cations, as well as one $\mathbf{L20}^{4-}$ unit in the structure of **42** are omitted for clarity.[87]

occurred with iodide or other polyatomic anions (ClO_4^-, NO_3^-, HCO_3^-, $H_2PO_4^-$, HSO_4^-, SO_4^{2-}), indicative of a high degree of preorganization of the $[Ni_2(\mathbf{L15}^{\mathbf{Me2H4}})]^{2+}$ cation and a size fit mismatch of the binding cavity of the complexes for anions larger than Br^-.

Interestingly, the variation of the nature of the coligand L′ had a strong influence on the magnetic properties of the $[Ni_2(\mathbf{L15}^{\mathbf{Me2H4}})(\mu\text{-L}')]^+$ complexes. In contrast to the fluorido-bridged complex, which featured a $S=0$ ground state, other halido- and pseudohalido-bridged complexes had a $S=2$ ground state that was attained by competing antiferromagnetic and ferromagnetic exchange interactions via the thiolato- and coligand bridges.

The electrochemical properties of the compounds reported in these studies agreed with those of other $Ni^{(II)}$ complexes supported by hexaaza dithiophenolato ligands. The $Ni^{(II)}/Ni^{(III)}$ redox potential correlated with the ligand field strength of the bridging coligand for the investigated halides. In this case, the ease of oxidation was paralleled by the position of the coligand in the spectrochemical series, i.e., $OH^- > Cl^- > F^-$.

The binding scheme of N_3^- was sensitive to the size of the macrocycle, as -$(CH_3)_3$- alkyl bridges ($[Ni_2(\mathbf{L15}^{\mathbf{Me2H4}})(\mu_{1,1}\text{-}N_3)]^+$) allowed this coligand to be bound in an $\mu_{1,1}$ fashion (end-on), while the binding motif is $\mu_{1,3}$ (end-to-end) for $[Ni_2(\mathbf{L14}^{\mathbf{R}})(\mu_{1,3}\text{-}N_3)]^+$. It is interesting to note that the Ni_2 complexes bridged by halides and pseudohalides displayed exclusively the conformation *B* (Figure 15).[68]

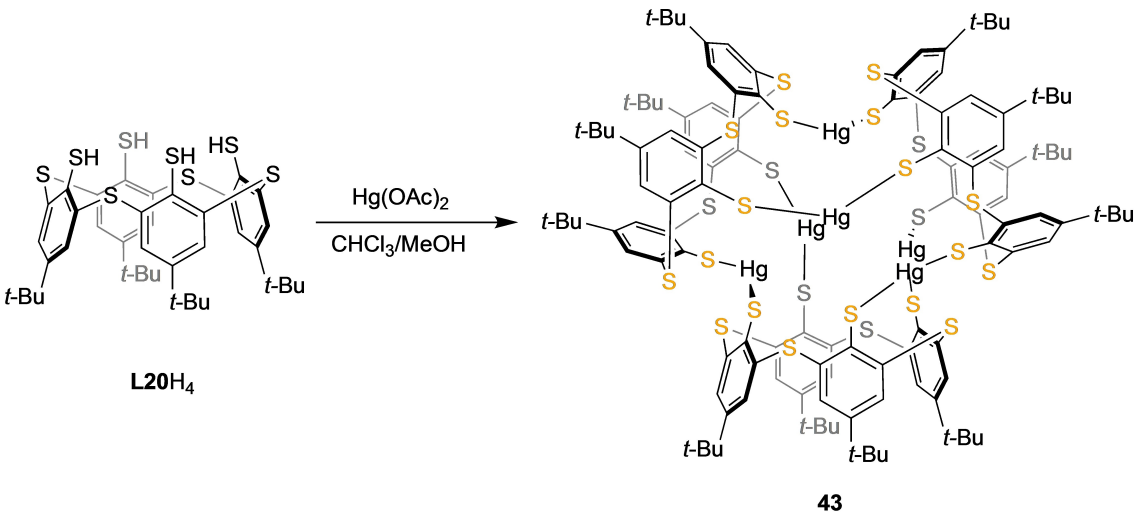

L20H_4

43

Figure 31. Bridging of three molecules of deprotonated tetrathiatetramercaptocalix[4]arenes **L20**$^{4-}$ by six Hg^{2+} cations by coordination to the arylthiolate sulfur anions to give the molecular assembly **43**.[88]

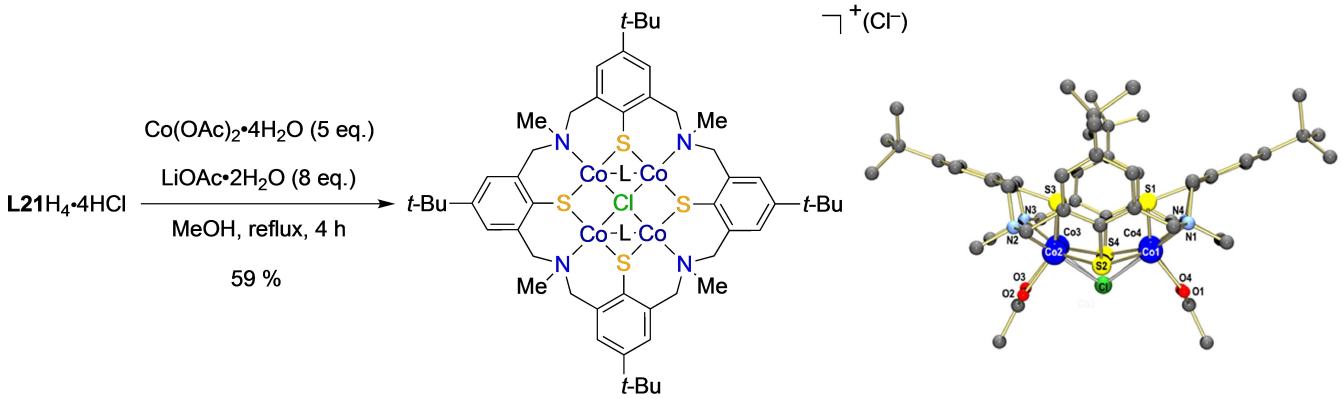

[Co_4(**L21**)(μ-Cl)(μ-OAc)$_2$]Cl

44

Figure 32. (Left) Preparation of the tetranuclear Co$^{(II)}$ complex **44** from the tetraazatetrathiacalix[4]arene **L21**H_4 (L=OAc$^-$); (right) ORTEP side view of the X-ray crystal structure of **44** (protons omitted for clarity).[89] (Reproduced from Ref. [89] Copyright (2022), with permission from Wiley-VCH GmbH).

4.4.2. Carboxylate-coligand functionalization with amine-based thiophenolate macrocyclic complexes

The coligands in [Ni_2(**L14**^{R})(L′)]$^{2+}$ are not limited to halides. Various alkyl- and aryl-carboxylates are also accommodated by this complex (Figure 17).[69] The dinuclear macrocyclic receptors hosted the carboxylato-coligands exclusively in the bowl-shaped conformation *A* of Figure 15.

Using a dicarboxylato-salen-complex as a linking unit, several dumbbell-shaped pentanuclear complexes **19** of the composition [{Ni_2([N6S2])}$_2$(μ-salen)M]$^{2+}$ with M being Ni$^{(II)}$, Cu$^{(II)}$, and Pd$^{(II)}$ were synthesized (Figure 18). Additionally, the use of the Pd$^{(II)}$ complex as a catalyst in the Heck reaction was investigated. However, due to the sterical hindrance of the central metal, the activity of this catalyst was low in comparison to other Pd-salen complexes.[70]

The complexation of some ambidentate mercapto-carboxylato ligands by [Ni_2(**L14**^{R})(Cl))]$^{2+}$ was examined. These ligands react with the Ni complex in a selective manner by substitution of the bridging chlorido ligand to produce exclusively $\mu_{1,3}$-carboxylato-bridged complexes. The resulting [Ni_2(**L14**^{R})(O_2C–R-SH)]$^+$ complexes can be utilized as paramagnetic metalloligands with a free thiol function. The complexes chemisorb on gold surfaces via the formation of covalent Au–S bonds, as established by contact-angle and XPS measurements.[71] More recently, the complexation of azobenzene-carboxylate-coligands was examined in order to obtain photoswitchable complexes. Irradiation of the Cd complex **22** (Figure 19) with a LED UV lamp leads to a *trans*-to-*cis* isomerization which proceeds within the binding pocket of the complex. The switch from the *trans* to the *cis* form induces significant changes of the π-π transitions of the supporting N_6S_2 macrocycle, which may

Review
doi.org/10.1002/ejic.202200739

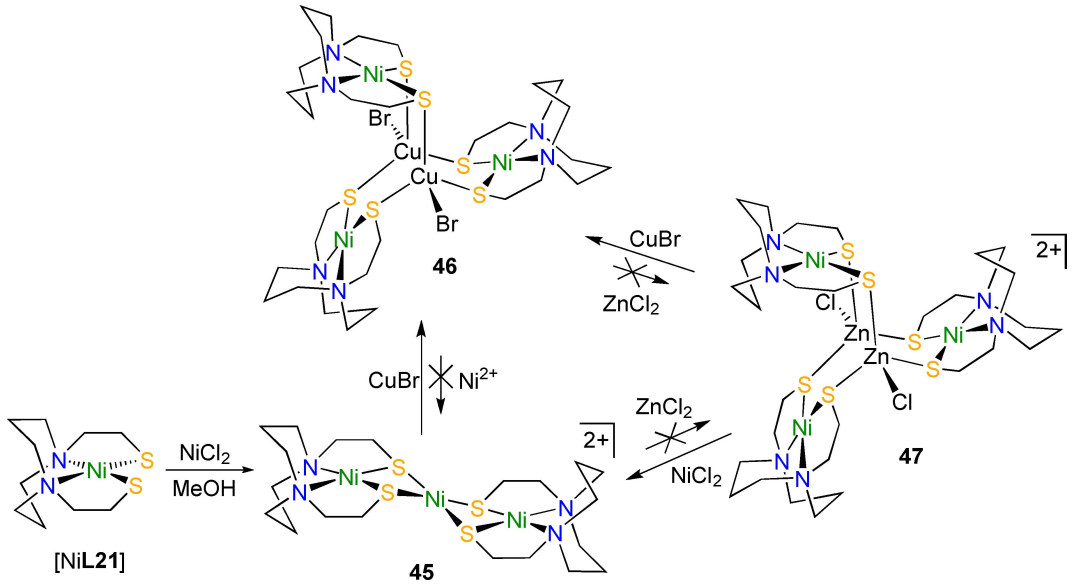

Figure 33. Reactions starting from a [N2S2] $Ni^{(II)}$ complex, which plays the role of metal-complex-as-ligand.[90]

be indicative of some increased π-π- (or charge transfer) interactions between the aromatic rings of the electron rich amino thiophenolato macrocycle and the electron poor azobenzene-carboxylato ligand. Photoswitchability was turned off when R = -OH, $-N(CH_3)_2$, $-CO_2CH_3$. Other metal cations, such as Zn^{2+} and Ni^{2+}, formed isostructural complexes of **22**, but they were not photoswitchable.[72]

4.4.3. Modification of the thiolate groups

Kersting and coworkers showed that $[Ni_2(\mathbf{L14^{Me}})O_2CR]^+$ reacted with molecular halides such as Br_2 and I_2 to form charge transfer (CT) complexes in which the dihalogen molecules were bound to one or two of the sulfur donors, depending on the nature of the carboxylate coligand (**23** and **24** of Figure 20).[73] The CT-compounds were relatively stable at ambient temperature with respect to the loss of gaseous I_2 and Br_2, respectively, due to the CT interactions between the thiolate sulfur atoms and the halide. In the solid state the iodine complex exhibited secondary I···I interactions with the enclathrated iodine molecules (or the polyiodide ions). In addition, intermolecular van der Waals attractions also contributed to the complex stability. These features confer a polymeric and less soluble nature on the iodine complexes.[68a,74] CT complexes from compartmental complexes based on the electron rich thiolate macrocycle $\mathbf{L14^{Me}}$ could be formed with Lewis acids as well. In the hexametallic complex **25**, for example, two $[Ni^{(II)}_2(\mathbf{L14^{Me}})(F)]^+$ complexes interact via their thiolate sulfur atoms with a central $Rh_2(OAc)_4$ unit (Figure 21). CT complexes **26** incorporating $Cu^{(I)}(halide)_2$ subunits could be obtained by reaction of $[Cu(X)_2]^-$ with $Ni^{(II)}$- and $Co^{(II)}$- containing $[M^{II}_2(\mathbf{L14^{Me}})(F)]^+$ complexes. The magnetic properties are greatly affected upon formation of the Lewis-acid/base complexes.[75]

4.4.4. S-oxygenation of macrocyclic amino-thiophenolato ligands

The oxygenation of metal thiolate complexes is of general interest with regard to the deactivation of metallocysteinate enzymes and the metabolism of cysteine. $[Ni_2(\mathbf{L14^{Me}})O_2CR]^+$ complexes are stable in air, both in solution and in solid state, which contrasts the behaviour of many other Ni thiolate complexes. Strong oxidants such as MCPBA or H_2O_2 were found to convert the thiolato to sulfonate complexes. Recently, α-ethereal hydroperoxides were also found to readily S-oxygenate the bridging thiophenolate functions (Figure 22). The reactions proceeded under ambient conditions without complex disintegration and invariably produced (S,O)-bridging sulfinate linkages.

Interestingly, conversion of the thiophenolate functions had a strong impact on the electronic structures of the nickel complexes. In the mixed thiolato/sulfinato complex **28**, the Ni^{2+} ions were ferromagnetically coupled as in the parent complex and produced a $S = 2$ spin ground state. Complex **29** exhibited an $S = 0$ ground state involving a weak antiferromagnetic exchange interaction.

It was suggested that the ether/O_2-mediated sulfoxygenation reaction of thiophenolate residues could also be applied to the synthesis of complexes for the modelling of metalloenzymes containing S-oxygenated cysteinate residues at their active sites as observed in cysteine dioxygenase (CDO), cysteamine dioxygenase (ADO), sulfoxide synthase (SO), nitrile hydratase (NHase), and NiFe hydrogenase enzymes.[20b,76]

Review
doi.org/10.1002/ejic.202200739

5. Complexation of $[MFe_3S_4]$ Clusters (M = Fe, Mo, V)

5.1. Subsite differentiation of cubane $[Fe_4S_4]$ clusters with tripod thiolate ligands

At a time when the X-ray crystal structures of the cofactors of the FeMoco, in particular the M cluster, were unknown, Holm and coworkers, relying on EXAFS data, designed a rigid tripod tri-thiol ligand **L16**H_3, into which could be inserted the vanadium and molybdenum cubane clusters $[VFe_3S_4]^{2+}$ and $[MoFe_3S_4]^{3+}$ **30** (Figure 23).[77] In the resulting complexes (e.g. **31**) the vanadium and the molybdenum cations are (sub)site-differentiated from the three iron cations, which allows them to undergo ligand exchange reactions, while the latter are "protected" by binding each to one of the three thiolate anions of **L16**$^{3-}$. The concept of subsite differentiation was extended to the $[Fe_4S_4]$ clusters themselves, in which one of the four iron cations could undergo non-cysteinate ligand substitution reactions. In addition to its fundamental interest, this work was motivated by the identification of non-redox metallo-enzymes, such as aconitase, that utilize an $[Fe_4S_4]$ cluster as a catalytic site. The site-differentiated iron cation could be bound to one anionic ligand (CN^-, N_3^-, OH^-, OMe^-, RS^-, OAc^-, ArX^-, X=O, S, and Se), dianonic chelates such as the catecholate, and accept up to three neutral ligands, monodentate such as isocyanide, and tridentate, such as TACN (Figure 24). Possible modes of protein binding were explored by binding of Cys-S^-, Tyr-O^-, Ser-O^- and Asp/Glu-CO_2^-. By contrast, the neutral imidazole and thioether residues of histidine and methionine did not coordinate the subsite-differentiated iron cation. The $[Fe_4S_4]^{2+/+}$ redox potentials, as well as the isotropic shifts of the protons of the tripod were shown to depend on the nature of the ligand bound to the subsite-differentiated iron atom. The substituents on the ArS^- metal binding arms were essential in controlling the 1:1 stoichiometry of the tripod/cluster complex, as the absence of substituents led to mixtures including polymers.[77d] Holm and coworkers also introduced a macrocyclic polyether tri-thiol derived from resorcinarene (**32**, see Figure 25a). As concluded by the authors, **32** could compete with **L16**H_3 for the complexation of $[Fe_4S_4]^-$ clusters and for their subsite differentiation.[78]

Other tri-thiolate ligands were designed that could perform the subsite differentiation of iron-sulfur clusters (Figure 25). Evans and coworkers[78] anchored three 4-mercaptobenzoyl subunits to 1,4,7-triazacyclononane (**33**) and 1,5,9-triazacyclododecane macrocyclic platforms to prepare subsite differentiated $[Fe_4S_4]$[79a] and $[MoFe_3S_4]$[79b] clusters. Nolte and coworkers took advantage of the cyclotribenzylene (CTB) platform (**34**) to investigate the effect of the nature and length of the spacers on the redox properties of the $[Fe_4S_4]$ cluster.[80] Remarkably, its orientation with respect to the concavity of the CTB depended on the nature of the ligand binding the differentiated Fe ion, the bulky *t*-BuS^- imposing an outward orientation, whereas the bound chloride strongly interacted with the electron-rich concavity.[80b] Saak and coworkers (Figure 25) introduced at that time a tripod ligand, 1,3,5-triethyl-2,4,6-tris(3-sulfanylindolyl[1]methyl)benzene **35**, which was easy to synthesize, and highly preorganized, as Holm's tripod.[81] Its persubstituted homologue, hexakis(3-sulfanylindolyl[1]methyl)benzene, could embed, after deprotonation, two $[Fe_4S_4]$ clusters at a rigid separation of 12.8 Å, as shown by single crystal XRD.[82]

5.2. Encapsulation of $[Fe_4S_4]$ clusters by tetrathiolate macrocycles and podands

Okuno and coworkers designed and used large-ring tetraazamacrocycles (**L17**^{R}, Figure 26) functionalized with four pendent thiol functional groups in order to investigate the effect of the hydrophobic environment provided by the protein backbone on the $[Fe_4S_4]$ cluster of high-potential iron-sulfur proteins (HiPIP). They observed that the clusters encapsulated in the tetraazamacrocycles (**L17**^{R}) had higher $[Fe_4S_4]^{2-/-}$ oxidation potentials and were less sensitive to dioxygen than their $[Fe_4S_4(SR)_4]^{2-}$ (R=Ph, Bn, and *t*-Bu) analogues, as in the case of the HiPIP clusters. This finding was very significant, because it showed that these properties were the consequence of the hydrophobic environment either provided by the protein or the macrocyclic backbones in the natural systems and their models, respectively.[83]

Tabushi and coworkers sandwiched an $[Fe_4S_4]$ cluster between two modified β-cyclodextrins, the 6 A and 6D alcohol functions of the small rim being replaced by *m*-$(SC_6H_4S^-)$ pendants (**36**, Figure 27). The resulting assembly had the unique property of being water-soluble and stable in aqueous solutions, enabling the authors to investigate the electrochemical properties of an $[Fe_4S_4]$ cluster in this medium.[84]

A tetrapod tetrathiolate thiolate ligand **37** based on the diphenylglycoluril concave platform was designed and used for a similar purpose by Nolte and coworkers (Figure 28). They observed that the electrochemical response of the encapsulated cluster was very weak, as in the case of the metalloproteins, and could be strongly enhanced by the addition of a modulator (Ba^{2+} or Na^+).[85]

5.3. Stabilization of high nuclearity [Fe-S] clusters by sterically-hindered monodentate thiolate ligands

It is interesting to note that sterically-hindered monodentate thiolate ligands can also stabilize high nuclearity iron-sulfur clusters, the topology of which is reminiscent of the topology of the P cluster of the nitrogenase.[86] The successive addition of stoichiometric amounts of **L18**H and **L19**H to $[Fe(NSiMe_3)_2]$ produced the dinuclear complex $[Fe^{(II)}_2(\mu\text{-}\mathbf{L18})_2(\mathbf{L19})_2]$ (**39**) in which the most sterically-hindered thiolate **L18**$^-$ bridged the Fe^{2+} cations, while the less sterically hindered thiolate **L19**$^-$ played the role of terminal ligand (Figure 29). The stabilization of the $[Fe_2S_2]$-type rhombs was due to the bulky thiolate substituents, which prevented them from oligomerization. The authors found that the reaction of **39** and 1/4S_8 in toluene gave

the cluster **40** [{Fe_4S_3(**L18**)}$_2$(μ-**L18**)$_2$(μ-**L19**)(μ_6-S)] in 28% yield. As in the case of the FeMoco, two incomplete [Fe_4S_3] cubane clusters were connected through a central atom (S^{2-} here vs. carbide in the natural system). The six central Fe cations of these cluster subunits were pairwise bridged by thiolate sulfur (one **L18**$^-$ and two **L19**$^-$vs. S^{2-} in the natural system), and the apical metal atoms connected to a thiolate sulfur (**L19**$^-$ vs. cysteine in the natural system). The [Fe_8S_7] cluster structure found in **40** might be a thermodynamically stable form, the formation of which competing favourably with the classical thermodynamic sink [Fe_4S_4] when the thiolate ligands are sterically hindered and when the solvents used are not polar.

6. Stabilization of High Nuclearity Metal-heteroatom Aggregates by Macrocycles

6.1. Tetramercaptotetrathiacalix[4]arene (L20H$_4$)

Tetramercaptotetrathiacalix[4]arene (**L20**H$_4$) is a macrocycle that can exhibit multiple conformations, depending on the relative orientations (cone, pinched-cone, 1,2-alternate, etc.) of the aromatic rings.[87] It offers a potential total of 8 monodentate binding sites, the four aromatic thioether bridges and the four aromatic thiolates obtained by deprotonation. Upon reaction of **L20**H$_4$ with 2/3 equiv. of the hexanuclear Cu$^{(I)}$ hydride (Cu-(PPh$_3$)H)$_6$ in toluene, the complex (Cu$_4$(PPh$_3$)$_4$**L20**) **41** was obtained, in which four [Cu(PPh$_3$)]$^+$ subunits bridged three consecutive sulfur atoms of **L20**H$_4$, each Cu$^{(I)}$ being located in a tetrahedral coordination environment (Figure 30).[87] In the solid state, the conformation of **L20**$^{4-}$ was the pinched-cone, but ^{1}H NMR studies in solution showed that the complex exhibited an average C_{4v} symmetry. When a metal precursor lacking the auxiliary PPh$_3$ ligand (e.g. the cluster [(Cu(NEt$_2$))$_4$]) was employed, a larger and more symmetrical metal-heteroatom aggregate was obtained, [(Cu$_4$**L20**)$_6$] (**42**). In this complex, the six **L20**$^{4-}$ crown ligands are arranged on the vertices of an octahedron owing to 24 bridging Cu$^+$ cations, each being surrounded by four sulfur atoms, one thioether and three thiolates, which provided each Cu$^+$ a tetrahedral coordination environment. Remarkably, the Cu$^+$ ions were arranged in [Cu_2S_2] diamond motifs, in which S was a thiolate sulfur, the Cu···Cu distance being 2.4725 Å, that is, shorter than in the reduced Cu$_A$ center (2.51 Å, see section 3c). Complexes **41** and **42** were related chemically, as reaction of the former with 24 equiv. of PPh$_3$ afforded the latter. An interesting peculiarity of **42** is the fact that the $Cu_{24}S_{48}$ aggregate is a hollow cage of ≈ 10 Å diameter and 187 Å^3 volume, which turned out to contain a diethylamine molecule, as shown by ^{1}H NMR studies.

The complex **42** was related to the Hg$_6$(**L20**)$_3$ complex **43**, the X-ray crystal structure of which had been reported earlier by Hosseini et al.[88] In the aggregate of the larger Hg^{2+} cations, three **L20**$^{4-}$ macrocycles in deformed cone conformation were arranged on the vertices of triangle, each calix[4]arene being bridged to its neighbour by two Hg^{2+} cations through coordination to the thiolate sulfur anions (Figure 31). The three pairs of Hg^{2+} were placed at the vertices of an almost perfect trigonal prism. Each Hg^{2+} was irregularly coordinated to six sulfur atoms, the shortest Hg–S bonds (2.38 and 2.41 Å) being those involving the two proximal thiolate sulfur, the other four sulfur atoms being at distances ranging from 2.95 to 3.06 Å. Although not noted by their authors, we believe that both of these works have a high significance as far as the biological role of metallothioneins (MTs) is concerned. As noted in the introduction, metallothioneins are low molecular weight and cystein-rich metal binding proteins, which are crucial for the Zn^{2+} and Cu$^+$ homeostasis, and which play an important part in metal detoxification by the sequestration of toxic soft heavy metal cations such as Cd^{2+}, Hg^{2+} and Pb^{2+}. Importantly, the affinity of the metallothioneins for soft metals follows the order: $Hg^{2+} > Ag^+ \sim Cu^+ > Cd^{2+} > Zn^{2+}$.[9b] Interestingly, the structure of the metallothionein from *Saccharomyces cerevisiae* (*S. cerevisiae* MT) could be determined by single crystal X-ray crystallography: 10 of the 12 cysteine residues (for a total of 53 aminoacids) were involved in Cu$^+$ coordination, in the form of a single [Cu_8(S(Cys))$_{10}$]$^{2-}$ cluster. Six Cu$^+$ feature a trigonal planar, and two a linear coordination geometry. Therefore the metal-sulfur aggregates **42** (Cu) and **43** (Hg) stabilized by the assembly of six and three molecules of calixarene **L20**$^{4-}$ are highly relevant as far as the mimicking of metallothioneins is concerned.

6.2. Tetraazatetrathiacalix[4]arene

We recently reported on the tetraazatetrathiacalix[4]arene **L21**H$_4$, which derives from calix[4]arene by substitution of the amine bridges for the methylene bridges, and can be considered as an expanded calixarene.[89] We showed that this macrocycle could form a tetranuclear Co$^{(II)}$ complex [Co_4(**L21**)(μ_4-Cl)(μ-OAc)$_2$]Cl (**44**), obtained in 59% yield after crystallisation, by reaction of **L21**H$_4$·4HCl with a slight excess of Co(OAc)$_2$·4H$_2$O in the presence of the stoichiometric amount of lithium acetate (Figure 32). An X-ray crystal structure determination showed that **L21**$^{4-}$ adopted a C_2-symmetric cone conformation in the complex, the four cobalt dications and a μ_4-bridging chloride anion closing the small opening of the calixarene. Each Co^{2+} ion is in a pentacoordinate trigonal bipyramidal coordination geometry, the apical donors being Cl$^-$ and the N atom of the closest bridging amine, the equatorial donors being two thiolate and an acetate anion. The discovery that macrocyclic ligands such as **L21**$^{4-}$ can host four redox-active metal cations in close proximity through thiolate coordination completed by the binding of the bridgehead nitrogen atoms and external anions (AcO$^-$ and Cl$^-$) suggests that these polymetallic complexes could be interesting to investigate as catalysts in multielectron transfer reactions to substrates bound via exchange of the acetate bridges.

6.3. Metallamacropolycycles

The square planar $Ni^{(II)}$ complex [Ni(**L22**)] was shown by Darensbourg and coworkers to mimic well the structure of the [N2S2]Ni complex subunit of ACS, by acting as a complex-as-ligand for $Ni^{(II)}$, $Cu^{(I)}$, and $Zn^{(II)}$ (Figure 33).[90] Indeed, reaction of two equiv. of [Ni(**L22**)] with $NiCl_2$ afforded the trinuclear complex $[(Ni(\mathbf{L22}))_2Ni]$ (**45**), while reaction of three equiv. of [Ni(**L22**)] with 2 equiv. of CuBr or $ZnCl_2$ afforded the pentanuclear complexes $[(Ni(\mathbf{L22}))_3(CuBr)_2]$ (**46**) and $[(Ni(\mathbf{L22}))_3(ZnCl)_2]^{2+}$ (**47**), respectively. The authors then explored the possibility to interconvert the three complexes into each other and found that whereas Cu^+ in complex **46** could not be replaced by either Zn^{2+} or Ni^{2+}, this was not the case for Zn^{2+} in complex **47**, which could be converted into either complex **46** or complex **45**. Cu^+ in complex **46** was a thermodynamic product, as Cu^+ could replace Ni^{2+} in complex **45** and Zn^{2+} in complex **47**.

7. Conclusion

This review has shown how the discovery of the structures of metallo-proteins involving cysteine amino-acid residues and inorganic sulfur as metal-binding subunits have stimulated the research on the coordination chemistry of metal cations with thiolate-functionalized ligands in the last fifty years. Thiolate is a soft monodentate ligand, which shows a strong propensity to bind two metal cations simultaneously. The nuclearity of the complexes was controlled by the architecture of the ligands. In particular, arylthiolates bearing sterically hindering substituents ortho to S^- were shown to stabilize mononuclear complexes, e.g. in which iron has a trigonal planar or a tetrahedral coordination geometry. Binuclear complexes could be obtained by using ligands, for example polyazamacrocycles, incorporating at least two thiolate subunits, which were preorganized in such a way that they could occupy opposite vertices of the M_2S_2 diamond. The use of open chain ligands bearing thiolate termini made it possible to prepare polynuclear complexes from metal-complexes-as-ligands. Higher nuclearities were obtained by using ligands containing several thiolate binding sites in combination with thioether, as observed in the case of tetrathiatetramercaptocalix[4]arene. However, the most fruitful approach to increase the nuclearity of the complexes was to combine the use of polythiolate ligands on one hand, and inorganic sulfide on the other hand, as exemplified by the so-called iron-sulfur clusters. Overall, the use of more complex thiolate ligands to construct polymetallic complexes has offered much potential for controlling structure, properties, and function, opening up new opportunities for fundamental studies and applications.

Despite the fascinating advances in this field, there remain many opportunities. For instance, stable heteropolynuclear thiolate complexes have great potential as biomimetic catalysts for hydrogen production, reduction of nitrogen to ammonia (nitrogenase) and oxidation of carbon monoxide to carbon dioxide (carbon monoxide dehydrogenase). Cooperation between redox-active metal centres and implementation of ligand-metal cooperativity in these complexes may be feasible and enable new catalytic reactions. There are also many opportunities to construct better-defined enzyme mimics, even second-sphere effects appear to be in reach.

Acknowledgements

Universität Leipzig, the Université de Strasbourg, and the CNRS are acknowledged for financial support. J. T. is grateful to the graduate school "BuildMoNa", and to the Embassy of France in Germany for a fellowship (PROCOPE Mobility Program).

Conflict of Interest

The authors declare no conflict of interest.

Data Availability Statement

The data that support the findings of this study are available from the corresponding author upon reasonable request.

Keywords: biomimetics · cluster compounds · coordination chemistry · macrocycles · S ligands

[1] E. I. Solomon, S. I. Gorelsky, A. Dey, *J. Comput. Chem.* **2006**, *27*, 1415–1428.
[2] N. D. J. Branscombe, A. J. Atkins, A. Marin-Becerra, E. J. L. McInnes, F. E. Mabbs, J. McMaster, M. Schröder, *Chem. Commun.* **2003**, 1098–1099.
[3] P. A. Stenson, A. Board, A. Marin-Becerra, A. J. Blake, E. S. Davies, C. Wilson, J. McMaster, M. Schröder, *Chem. Eur. J.* **2008**, *14*, 2564–2576.
[4] A. J. Atkins, D. Black, A. J. Blake, A. Marin-Becerra, S. Parsons, L. Kuiz-Ramirezc, M. Schröder, *Chem. Commun.* **1996**, 457–464.
[5] I. G. Dance, *Polyhedron* **1986**, *5*, 1037–1104.
[6] A. J. Amoroso, S. S. M. Chung, D. J. E. Spencer, J. P. Danks, M. W. Glenny, A. J. Blake, P. A. Cooke, C. Wilson, M. Schröder, *Chem. Commun.* **2003**, 2020–2021.
[7] M. T. Chaudhry, S. Akine, M. J. MacLachlan, *Chem. Soc. Rev.* **2021**,*50*, 10713–10732.
[8] S. Brooker, *Coord. Chem. Rev.* **2001**, *222*, 33–56.
[9] a) G. Isani, E. Carpenè, *Biomol. Eng.* **2014**, *4*, 435–457; b) J. Calvo, H. Jung, G. Meloni, *IUBMB Life* **2017**, *69*, 236–245.
[10] a) T. A. Rouault, *Nat. Reviews* **2015**, *16*, 45–55; b) J. Liu, S. Chakraborty, P. Hosseinzadeh, Y. Yu, S. Tian, I. Petrik, A. Bhagi, Y. Lu, *Chem. Rev.* **2014**, *114*, 4366–4469.
[11] W. Lubitz, H. Ogata, O. Rüdiger, E. Reijerse, *Chem. Rev.* **2014**, *114*, 4081–4148.
[12] I. G. Denisov, T. M. Makris, S. G. Sligar, I. Schlichting, *Chem. Rev.* **2005**, *105*, 2253–2277.
[13] Y. Sheng, I. A. Abreu, D. E. Cabelli, M. J. Maroney, A.-F. Miller, M. Teixeira, J. S. Valentine, *Chem. Rev.* **2014**, *114*, 3854–3918.
[14] M. Can, F. A. Armstrong, S. W. Ragsdale, *Chem. Rev.* **2014**, *114*, 4149–4174.
[15] S. R. Pauleta, S. Dell'Acqua, I. Moura, *Coord. Chem. Rev.* **2013**, *257*, 332–349.
[16] a) J. Kim, D. C. Rees, *Nature* **1992**, *360*, 553–560; b) J. Kim, D. C. Rees, *Biochemistry* **1994**, *33*, 389–397.
[17] K. H. Hopmann, *Inorg. Chem.* **2014**, *53*, 2760–2762.
[18] B. V. Plapp, B. R. Savarimuthu, D. J. Ferraro, J. K. Rubach, E. N. Brown, S. Ramaswamy, *Biochemistry* **2017**, *56*, 3632–3646.

[19] a) J. B. Howard, D. C. Rees, *Chem. Rev.* **1996**, *96*, 2965–2982; b) O. Einsele, F. A. Tezcan, S. L. A. Andrade, B. Schmid, M. Yoshida, J. B. Howard, D. C. Rees, *Science* **2002**, *297*, 1696–1700.
[20] a) E. Bouwman, J. Reedijk, *Coord. Chem. Rev.* **2005**, *249*, 1555–1581; b) C. Tard, C. J. Pickett, *Chem. Rev.* **2009**, *109*, 2245–2274; c) Y. Ohki, K. Tatsumi, *Eur. J. Inorg. Chem.* **2011**, *2011*, 973–985; d) J. A. Denny, M. Y. Darensbourg, *Chem. Rev.* **2015**, *115*, 5248–5273; e) T. R. Simmons, G. Berggren, M. Bacchi, M. Fontecave, V. Artero, *Coord. Chem. Rev.* **2014**, *270–271*, 127–150; f) N. Khadka, R. D. Milton, S. Shaw, D. Lukoyanov, D. R. Dean, S. D. Minteer, S. Raugei, B. M. Hoffman, L. C. Seefeldt, *J. Am. Chem. Soc.* **2017**, *139*, 13518–13524.
[21] B. K. Maiti, R. M. Almeida, I. Moura, J. J. G. Moura, *Coord. Chem. Rev.* **2017**, *352*, 379–397.
[22] M. Corsini, P. Zanello, *Inorganics* **2022**, *10*, 14.
[23] A. Albers, T. Bayer, S. Demeshko, S. Dechert, F. Meyer, *Chem. Eur. J.* **2013**, *19*, 10101–10106.
[24] P. Bonora, I. Principi, B. Monti, S. Ciurli, D. Zannoni, A. Hochkoeppler, *Biochim. Biophys. Acta* **1999**, *1410*, 51–60.
[25] J. C. Fontecilla-Camps, A. Volbeda, *Chem. Rev.* **2022**, *122*, 12110–12131.
[26] B. A. Averill, *Chem. Rev.* **1996**, *96*, 2951–2964.
[27] a) A. S. Pandey, T. V. Harris, L. J. Giles, J. W. Peters, R. K. Szilagyi, *J. Am. Chem. Soc.* **2008**, *130*, 4533–4540; b) K. Parey, E. Warkentin, P. M. H. Kroneck, U. Ermler, *Biochemistry* **2010**, *49*, 8912–8921.
[28] J. T. Kleinhaus, F. Wittkamp, S. Yadav, D. Siegmund, U.-P. Apfel, *Chem. Soc. Rev.* **2021**, *50*, 1668–1784.
[29] a) V. Svetlitchnyi, H. Dobbek, W. Meyer-Klaucke, T. Meins, B. Thiele, P. Römer, R. Huber, O. Meyer, *Proc. Nat. Acad. Sci. USA* **2004**, *101*, 446–451; b) J. C. Fontecilla-Camps, A. Volbeda, C. Cavazza, Y. Nicolet, *Chem. Rev.* **2007**, *107*, 4273–4303.
[30] E. L. Hegg, *Acc. Chem. Res.* **2004**, *37*, 775–783.
[31] a) J. B. Howard, D. C. Rees, *Chem. Rev.* **1996**, *96*, 2965–2982; b) H. Schindelin, C. Kisker, J. L. Schlessman, J. B. Howard, D. C. Rees, *Nature* **1997**, *387*, 370–376; c) J. W. Peters, M. H. B. Stowell, S. M. Soltis, M. G. Finnegan, M. K. Johnson, D. C. Rees, *Biochemistry* **1997**, *36*, 1181–1187; d) S. M. Mayer, D. M. Lawson, C. A. Gormal, S. M. Roe, B. E. Smith, *J. Mol. Biol.* **1999**, *292*, 871–891; e) L.-M. Zhang, C. N. Morrison, J. T. Kaiser, D. C. Rees, *Acta Crystallogr.* **2015**, *D71*, 274–282; f) S. Burén, E. Jiménez-Vicente, C. Etchavarri-Erasun, L. M. Rubio, *Chem. Rev.* **2020**, *120*, 4921–4968; g) O. Einsle, D. C. Rees, *Chem. Rev.* **2020**, *120*, 4969–5004; h) C. Van Stappen, L. Decamps, G. E. Cutsail III, R. Bjornsson, J. T. Henthorn, J. A. Birrell, S. DeBeer, *Chem. Rev.* **2020**, *120*, 5005–5081; i) L. C. Seefeldt, Z.-Y. Yang, D. A. Lukoyanov, D. F. Harris, D. R. Dean, S. Raugei, B. M. Hoffman, *Chem. Rev.* **2020**, *120*, 5082–5106; j) A. J. Janiewski, C. C. Lee, M. W. Ribbe, Y. Hu, *Chem. Rev.* **2020**, *120*, 5107–5157; k) H. L. Rutledge, F. A. Tezcan, *Chem. Rev.* **2020**, *120*, 5158–5193; l) X. Zhang, B. B. Ward, D. M. Sigman, *Chem. Rev.* **2020**, *120*, 5308–5351.
[32] a) T. Spatzal, M. Aksoyoglu, L. M. Zhang, S. L. A. Andrade, E. Schleicher, S. Weber, D. C. Rees, O. Einsle, *Science* **2011**, *334*, 940; b) K. M. Lancaster, M. Roemelt, P. Ettenhuber, Y. Hu, M. W. Ribbe, F. Neese, U. Bergmann, S. DeBeer, *Science* **2011**, *334*, 974–977.
[33] G. Moula, A. Nagasaki, T. Matsumoto, M. E. Miehlich, K. Meyer, R. E. Cramer, K. Tatsumi, *Angew. Chem. Int. Ed.* **2021**, *60*, 15792–15797.
[34] a) H. Deng, R. Hoffmann, *Angew. Chem. Int. Ed.* **1993**, *32*, 1062–1065; b) B. K. Burgess, D. J. Lowe, *Chem. Rev.* **1996**, *96*, 2983–3011; c) B. M. Hoffman, D. Lukoyanov, Z.-Y. Yang, D. R. Dean, L. C. Seefeldt, *Chem. Rev.* **2014**, *114*, 4041–4062; d) P. E. M. Siegbahn, *Phys. Chem. Chem. Phys.* **2019**, *21*, 15747–15759; e) T. M. Buscagan, D. C. Rees, *Joule* **2019**, *3*, 2662–2678.
[35] M. Gennari, C. Duboc, *Acc. Chem. Res.* **2020**, *53*, 2753–2761.
[36] P. V. Rao, R. H. Holm, *Chem. Rev.* **2004**, *104*, 527–559.
[37] F. M. MacDonnell, K. Ruhlandt-Senge, J. J. Ellison, R. H. Holm, P. P. Power, *Inorg. Chem.* **1995**, *34*, 1815–1822.
[38] M. Millar, J. F. Lee, T. O'Sullivan, S. A. Koch, R. Fikar, *Inorg. Chim. Acta* **1996**, *243*, 333–343.
[39] I. Čorić, B. Q. Mercado, E. Bill, D. J. Vinyard, P. L. Holland, *Nature* **2015**, *526*, 96–99.
[40] A. L. Speelman, I. Čorić, C. Van Stappen, S. DeBeer, B. Q. Mercado, P. L. Holland, *J. Am. Chem. Soc.* **2019**, *141*, 13148–13157.
[41] N. Govindaswamy, D. A. Quarless, S. A. Koch, *J. Am. Chem. Soc.* **1995**, *117*, 8468–8469.
[42] D. H. Nguyen, H.-F. Hsu, M. Millar, S. A. Koch, C. Achim, E. L. Bominaar, E. Münck, *J. Am. Chem. Soc.* **1996**, *118*, 8963–8964.
[43] H.-F. Hsu, S. A. Koch, C. V. Popescu, E. Münck, *J. Am. Chem. Soc.* **1997**, *119*, 8371–8372.
[44] W.-C. Chu, C.-C. Wu, H.-F. Hsu, *Inorg. Chem.* **2006**, *45*, 3164–3166.
[45] Y.-H. Chang, P.-M. Chan, Y.-F. Tsai, G.-H. Lee, H.-F. Hsu, *Inorg. Chem.* **2014**, *53*, 664–666.
[46] a) A. M. Pujol, C. Gateau, C. Lebrun, P. Delangle, *J. Am. Chem. Soc.* **2009**, *131*, 6928–6929; b) A. M. Pujol, M. Cuillel, O. Renaudet, C. Lebrun, P. Charbonnier, D. Cassio, C. Gateau, P. Dumy, E. Mintz, P. Delangle, *J. Am. Chem. Soc.* **2011**, *133*, 286–296; c) A.-S. Jullien, C. Gateau, I. Kieffer, D. Testemale, P. Delangle, *Inorg. Chem.* **2013**, *52*, 9954–9961.
[47] a) B. M. Bridgewater, G. Parkin, *Inorg. Chem. Commun.* **2001**, *4*, 126–129; b) M. M. Morlok, K. E. Janak, G. Zhu, D. A. Quarless, G. Parkin, *J. Am. Chem. Soc.* **2005**, *127*, 14039–14050.
[48] D. Sellmann, W. Soglowek, F. Knoch, M. Moll, *Angew. Chem. Int. Ed. Engl.* **1989**, *28*, 1271–1272.
[49] Y. Zhu, D. O. V. Alonso, K. Maki, C. Y. Huang, S. J. Lahr, V. Daggett, H. Roder, W. F. DeGrado, F. Gai, *Proc. Natl. Acad. Sci. USA* **2003**, *100*, 15486–15491.
[50] S. Chakraborty, J. Y. Kravitz, P. W. Thulstrup, L. Hemmingsen, W. F. DeGrado, V. L. Pecoraro, *Angew. Chem. Int. Ed. Engl.* **2011**, *50*, 2049–2053.
[51] D. Yang, Y. Li, B. Wang, X. Zhao, L. Su, S. Chen, P. Tong, Y. Luo, J. Qu, *Inorg. Chem.* **2015**, *54*, 10243–10249.
[52] a) Y. Chen, Y. Zhou, P. Chen, Y. Tao, Y. Li, J. Qu, *J. Am. Chem. Soc.* **2008**, *130*, 15250–15251; b) Y. Chen, L. Liu, Y. Peng, P. Chen, Y. Luo, J. Qu, *J. Am. Chem. Soc.* **2011**, *133*, 1147–1149.
[53] M. Yuki, K. Sakata, Y. Hirao, N. Nonoyama, K. Nakajima, Y. Nishibayashi, *J. Am. Chem. Soc.* **2015**, *137*, 4173–4182.
[54] M. Gennari, J. Pecaut, S. DeBeer, F. Neese, M. N. Collomb, C. Duboc, *Angew. Chem. Int. Ed. Engl.* **2011**, *50*, 5662–5666.
[55] T. Beissel, T. Glaser, F. Kesting, K. Wieghardt, B. Nuber, *Inorg. Chem.* **1996**, *35*, 3936–3947.
[56] A. C. Marr, D. J. E. Spencer, M. Schröder, *Coord. Chem. Rev.* **2001**, *219*, 1055–1074.
[57] M. van Gastel, J. L. Shaw, A. J. Blake, M. Flores, M. Schröder, J. McMaster, W. Lubitz, *Inorg. Chem.* **2008**, *47*, 11688–11697.
[58] J. Dawson, C. Perotto, J. McMaster, M. Schröder, *[NiFe] Hydrogenases, in „Bioinspired Catalysis"*, ed W. Weigand, P. Schollhammer, Wiley-VCH, Weinheim, **2014**, 49–78.
[59] N. H. Pilkington, R. Robson, *Aust. J. Chem.* **1970**, *23*, 2225–2236.
[60] S. Brooker, P. D. Croucher, T. C. Davidson, G. S. Dunbar, C. U. Beck, S. Subramanian, *Eur. J. Inorg. Chem.* **2000**, 169–179.
[61] B. Kersting, G. Steinfeld, *Chem. Commun.* **2001**, 1376–1377.
[62] a) B. Kersting, D. Siebert, D. Volkmer, M. J. Kolm, C. Janiak, *Inorg. Chem.* **1999**, *38*, 3871–3882; b) B. Kersting, D. Siebert, *Inorg. Chem.* **1998**, *37*, 3820–3828.
[63] a) V. Lozan, C. Loose, J. Kortus, B. Kersting, *Coord. Chem. Rev.* **2009**, *253*, 2244–2260; b) M. Börner, J. Klose, M. E. Gutierrez Suburu, C. A. Strassert, F. Yang, K. Y. Monakhov, B. Abel, B. Kersting, *Chem. Eur. J.* **2021**, *27*, 14899–14910; c) Y. Journaux, V. Lozan, J. Klingele, B. Kersting, *Chem. Commun.* **2006**, 83–84.
[64] J. Lach, A. Jeremies, V. Lozan, C. Loose, T. Hahn, J. Kortus, B. Kersting, *Inorg. Chem.* **2012**, *51*, 12380–12388.
[65] J. A. Seddon, A. R. W. Jackson, R. A. Kresiński, A. W. G. Platt, *J. Chem. Soc. Dalton Trans.* **1999**, 2189–2196.
[66] M. Yoshizawa, T. Kusukawa, M. Fujita, K. Yamaguchi, *J. Am. Chem. Soc.* **2000**, *122*, 6311–6312.
[67] B. Kersting, G. Steinfeld, *Inorg. Chem.* **2002**, *41*, 1140–1150.
[68] a) A. Jeremies, U. Lehmann, S. Gruschinski, V. Matulis, O. A. Ivashkevich, A. Jäschke, B. Kersting, *J. Organomet. Chem.* **2016**, *821*, 171–181; b) A. Jeremies, S. Gruschinski, S. Schmorl, T. Severin, B. Kersting, *New J. Chem.* **2018**, *42*, 7630–7639.
[69] B. Kersting, *Angew. Chem.* **2001**, *113*, 4110–4112; *Angew. Chem. Int. Ed.* **2001**, *40*, 3988–3990.
[70] M. Golecki, B. Kersting, *Z. Anorg. Allg. Chem.* **2015**, *641*, 436–441.
[71] M. Börner, L. Blomer, M. Kischel, P. Richter, G. Salvan, D. R. T. Zahn, P. F. Siles, M. E. N. Fuentes, C. C. B. Bufon, D. Grimm, O. G. Schmidt, D. Breite, B. Abel, B. Kersting, *Beilstein J. Nanotechnol.* **2017**, *8*, 1375–1387.
[72] J. Klose, T. Severin, P. Hahn, A. Jeremies, J. Bergmann, D. Fuhrmann, J. Griebel, B. Abel, B. Kersting, *Beilstein J. Org. Chem.* **2019**, *15*, 840–851.
[73] M. Golecki, N. Beyer, G. Steinfeld, V. Lozan, S. Voitekhovich, M. Sehabi, J. Möllmer, H.-J. Krüger, B. Kersting, *Angew. Chem.* **2014**, *126*, 10107–10111; *Angew. Chem. Int. Ed.* **2014**, *37*, 9949–9952.
[74] a) G. Steinfeld, V. Lozan, H. J. Kruger, B. Kersting, *Angew. Chem. Int. Ed. Engl.* **2009**, *48*, 1954–1957; b) N. Beyer, G. Steinfeld, V. Lozan, S. Naumov, R. Flyunt, B. Abel, B. Kersting, *Chem. Eur. J.* **2017**, *23*, 2303–2314.

[75] a) S. Schmorl, M. Börner, B. Kersting, *Dalton Trans.* **2021**, *51*, 59–62; b) S. Schmorl, S. Naumov, B. Abel, M. Börner, A. Poppl, B. Kersting, *Dalton Trans.* **2021**, *50*, 5784–5788.
[76] M. Borner, D. Fuhrmann, J. Klose, H. Krautscheid, B. Kersting, *Inorg. Chem.* **2021**, *60*, 13517–13527.
[77] a) T. D. P. Stack, R. H. Holm, *J. Am. Chem. Soc.* **1987**, *109*, 2546–2547; b) T. D. P. Stack, R. H. Holm, *J. Am. Chem. Soc.* **1988**, *110*, 2484–2494; c) S. Ciurli, R. H. Holm, *Inorg. Chem.* **1989**, *28*, 1685–1690; d) T. D. P. Stack, J. A. Weigel, R. H. Holm, *Inorg. Chem.* **1990**, *29*, 3745–3760.
[78] M. A. Whitener, G. Peng, R. H. Holm, *Inorg. Chem.* **1991**, *30*, 2411–2417.
[79] a) D. J. Evans, G. Garcia, G. J. Leigh, M. S. Newton, M. D. Santana, *J. Chem. Soc. Dalton Trans.* **1992**, 3229–3234; b) J. E. Barclay, D. J. Evans, G. Garcia, M. D. Santana, M. C. Torralba, J. M. Yago, *J. Chem. Soc. Dalton Trans.* **1995**, 1965–1971.
[80] a) G. P. F. van Strijdonck, J. A. E. H. van Haare, J. G. M. van der Linden, J. J. Steggerda, R. J. M. Nolte, *Inorg. Chem.* **1994**, *33*, 999–1000; b) G. P. F. van Strijdonck, J. A. E. H. Van Haare, P. J. M. Hönen, R. C. G. M. van den Schoor, M. C. Feiters, J. G. M. van der Linden, J. J. Steggerda, R. J. M. Nolte, *J. Chem. Soc. Dalton Trans.* **1997**, 449–462.
[81] C. Walsdorff, W. Saak, S. Pohl, *J. Chem. Soc. Dalton Trans.* **1997**, 1857–1862.
[82] C. Walsdorff, W. Saak, *Chem. Commun.* **1997**, 1931–1932.
[83] a) Y. Okuno, K. Uoto, Y. Sasaki, O. Yonemitsu, T. Tomohiro, *J. Chem. Soc. Chem. Commun.* **1987**, 874–876; b) Y. Okuno, K. Uoto, O. Yonemitsu, T. Tomohiro, *J. Chem. Soc. Chem. Commun.* **1987**, 1018–1020; c) H. Okuno, K. Uoto, T. Tomohiro, M.-T. Youinou, *J. Chem. Soc. Dalton Trans.* **1990**, 3375–3381.
[84] Y. Kuroda, Y. Sasaki, Y. Shiroiwa, I. Tabushi, *J. Am. Chem. Soc.* **1988**, *110*, 4049–4050.
[85] C. F. Martens, H. L. Blonk, T. Bongers, J. G. M. van der Linden, G. Beurskens, P. T. Beurskens, J. M. M. Smits, R. J. M. Nolte, *J. Chem. Soc. Chem. Commun.* **1991**, 1623–1625.
[86] a) Y. Ohki, Y. Ikagawa, K. Tatsumi, *J. Am. Chem. Soc.* **2007**, *129*, 10457–10465; b) T. Hashimoto, Y. Ohki, K. Tatsumi, *Inorg. Chem.* **2010**, *49*, 6102–6109.
[87] N. Frank, A. Dallmann, B. Braun-Cula, C. Herwig, C. Limberg, *Angew. Chem. Int. Ed.* **2020**, *59*, 6735–6739.
[88] H. Akdas, E. Graf, M. W. Hosseini, A. De Cian, A. Bilyk, B. W. Skelton, G. A. Koutsantonis, J. Murray, J. M. Harrowfield, A. H. White, *Chem. Commun.* **2002**, 1042–1043.
[89] F. Schleife, C. Bonnot, J.-C. Chambron, M. Börner, B. Kersting, *Chem. Eur. J.* **2022**, *28*, e202104255.
[90] M. L. Golden, M. V. Rampersad, J. H. Reibenspies, M. Y. Darensbourg, *Chem. Commun.* **2003**, 1824–1825.

Manuscript received: November 30, 2022
Revised manuscript received: February 3, 2023

REVIEW

This review shows, with selected examples, how the evolution of the coordination chemistry of transition metal cations with thiolate-based ligands paralleled, at least in part, the concomitant development of bioinorganic chemistry during the last 50 years, with emphasis on the strategies directed at the controlled and reproducible synthesis of multimetallic thiolate complexes.

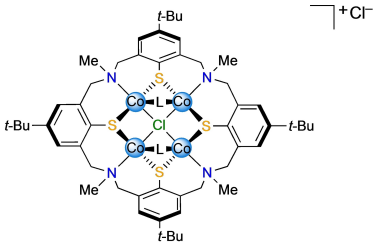

$[Co_4([N4S4]calix[4]arene)(\mu\text{-}Cl)(\mu\text{-}OAc)_2]Cl$

J. Taut, Dr. J.-C. Chambron, Prof. Dr. B. Kersting**

1 – 25

Fifty Years of Inorganic Biomimetic Chemistry: From the Complexation of Single Metal Cations to Polynuclear Metal Complexes by Multidentate Thiolate Ligands